How to cite: *Angew. Chem. Int. Ed.* **2024**, *63*, e202311241
doi.org/10.1002/anie.202311241

Metal-Organic Frameworks

Selective Gas-Phase Hydrogenation of CO_2 to Methanol Catalysed by Metal-Organic Frameworks

Amarajothi Dhakshinamoorthy, Sergio Navalón, Ana Primo, and Hermenegildo García**

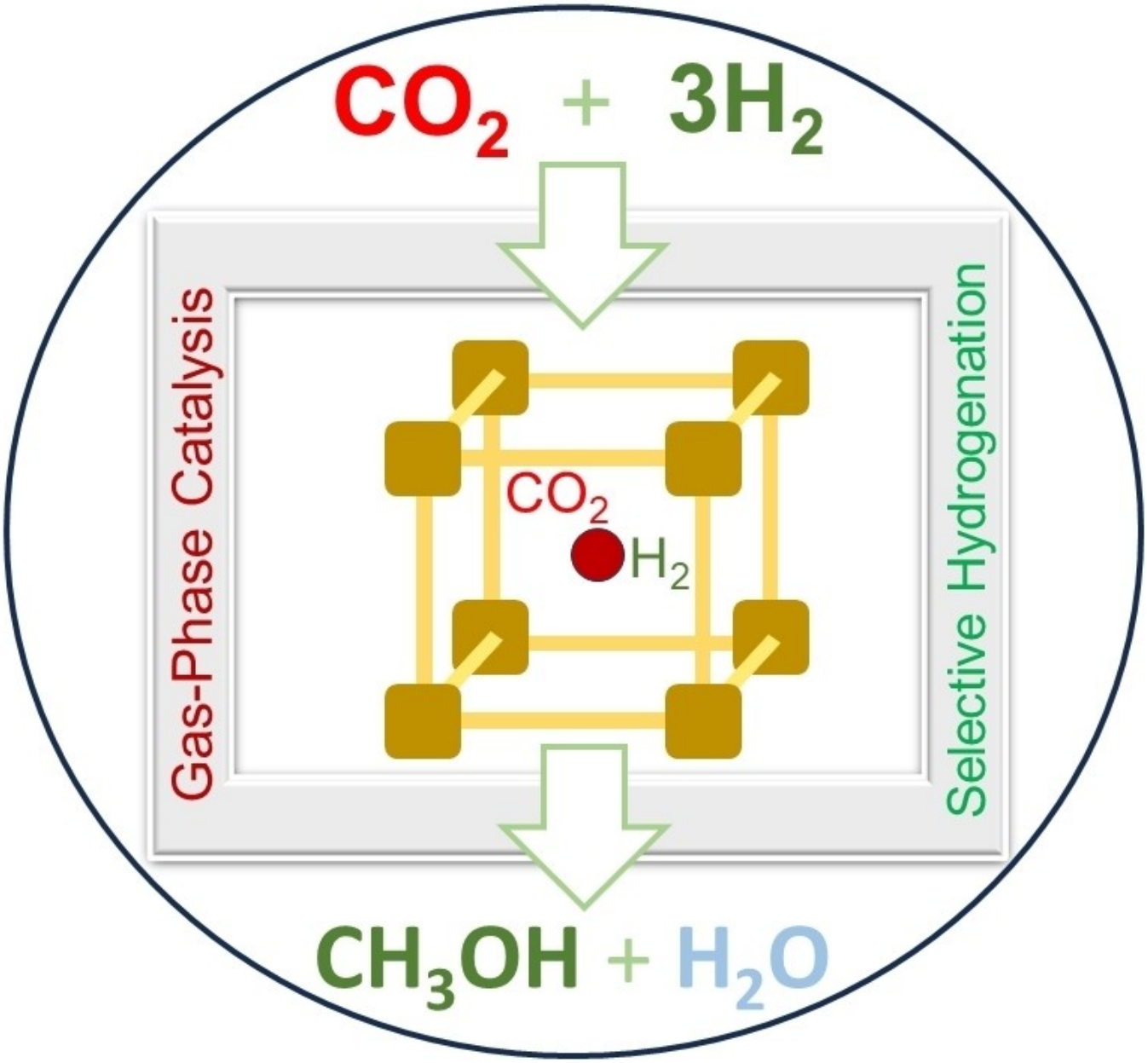

Abstract: Large scale production of green CH_3OH obtained from CO_2 and green H_2 is a highly wanted process due to the role of CH_3OH as H_2/energy carrier and for producing chemicals. Starting with a short summary of the advantages of metal–organic frameworks (MOFs) as catalysts in liquid-phase reactions, the present article highlights the opportunities that MOFs may offer also for some gas-phase reactions, particularly for the selective CO_2 hydrogenation to CH_3OH. It is commented that there is a temperature compatibility window that combines the thermal stability of some MOFs with the temperature required in the CO_2 hydrogenation to CH_3OH that frequently ranges from 250 to 300 °C. The existing literature in this area is briefly organized according to the role of MOF as providing the active sites or as support of active metal nanoparticles (NPs). Emphasis is made to show how the flexibility in design and synthesis of MOFs can be used to enhance the catalytic activity by adjusting the composition of the nodes and the structure of the linkers. The influence of structural defects and material crystallinity, as well as the role that should play theoretical calculations in models have also been highlighted.

1. Introduction

Since green CH_3OH is considered as a potentially clean fuel and one of the important raw materials to produce a wide range of chemicals,[1–4] the development of a suitable and efficient chemical process for the synthesis of CH_3OH from CO_2 has become a key reaction in the new H_2 technology sector.[5–7] To achieve this transformation, a ternary Cu/ZnO/Al_2O_3 catalyst industrially employed for the syn gas (CO/H_2) synthesis of CH_3OH has also been proposed as a benchmark catalyst for the selective CO_2 hydrogenation to CH_3OH.[8,9] However, the catalytic activity of $Cu/ZnO/Al_2O_3$ is still not fully satisfactory due to deactivation and there are also some mechanistic details related to the real nature of active sites that are still unclear. The current understanding points to the key role played by Cu/ZnOx interface.[10–12]

Hu and co-workers have reported the activity of MoS_2 in the hydrogenation of CO_2 to CH_3OH and this activity was proposed to derive from in-plane sulfur vacancies in MoS_2 nanosheets.[13] Besides MoS_2, In_2O_3 has also been effectively employed as an efficient catalyst for the hydrogenation of CO_2 to CH_3OH and the mostly accepted active sites in this solid are the oxygen vacancies on its surface that further play the vital role in determining the high selectivity and activity to CH_3OH.[14–17] These precedents have shown that the activity of In_2O_3 is superior compared to Cu, Co, or noble metals as well as ZnO catalyst. Furthermore, the activity of In_2O_3 can be easily modified by supporting other active sites to facilitate the activation of both CO_2 and H_2 and stabilizing the key intermediates, thus constituting a promising material for the sustainable CH_3OH production.[18–22] On the other hand, atomically dispersed Pd over ZnZrOx to obtain Pd–ZnZrOx solid solution and its performance was reported in the production of CH_3OH. Interestingly, the activity of Pd–ZnZrOx was superior compared to bare ZnZrOx and the stability of the former solid is also reported over 100 h on stream.[23]

As commented earlier, $Cu/ZnO/Al_2O_3$ and other metal oxides have been widely employed as heterogeneous solid catalysts for the hydrogenation of CO_2 to CH_3OH. However, one of the key issues in this conversion is to precisely determine the nature of reaction intermediates as well as to identify the reaction pathway. In general, there are two mechanisms that are widely accepted for this transformation using Cu/ZnO as a catalyst (Scheme 1).[24] One of the mechanistic pathways is called formate mechanism (a) in where CO_2 hydrogenation proceeds through the formation of adsorbed formate intermediates (HCOO*), and other route involves the reverse water-gas-shift (RWGS) and CO hydrogenation mechanism (b), where CO_2 is transformed initially to CO which may react by hydrogenation to CH_3OH via adsorbed formyl (HCO*) and formaldehyde (HCHO*) intermediates.[25–28] These different reactions are summarized in Scheme 1.

Metal–organic frameworks (MOFs) have been among the most researched heterogeneous catalysts for liquid phase reactions in the last decades.[30–33] There are multitude of reviews summarizing the state of the art regarding the activity, nature of active sites and strategies to increase the performance of these solid catalysts.[34,35] The major reasons for the wide interest on MOFs as solid catalysts in liquid phase are the wide range of compositions respect to the transition metals and the organic linkers, the flexibility in design and synthesis, the large density of active sites,[33,36] multifunctionality,[37] as well as the large porosity and specific surface area of these materials.[38–40] Active sites in MOFs can be exchangeable coordination positions around the metal nodes,[41] frequently occupied by easily removable solvent molecules or water, as well as functional groups on the organic linkers[42] or even active molecular complexes or NPs hosted within the internal pores. Since MOFs can be

[*] A. Dhakshinamoorthy, S. Navalón
Departamento de Química, Universitat Politècnica de València
Camino de Vera s/n, Valencia 46022 (Spain)
E-mail: admguru@gmail.com
sernaol@doctor.upv.es

A. Dhakshinamoorthy
School of Chemistry, Madurai Kamaraj University
Madurai 625021 Tamil Nadu (India)

A. Primo, H. García
Instituto Universitario de Tecnología Química, CSIC-UPV, Universitat Politècnica de València
Camino de Vera s/n, Valencia 46022 (Spain)
E-mail: hgarcia@qim.upv.es

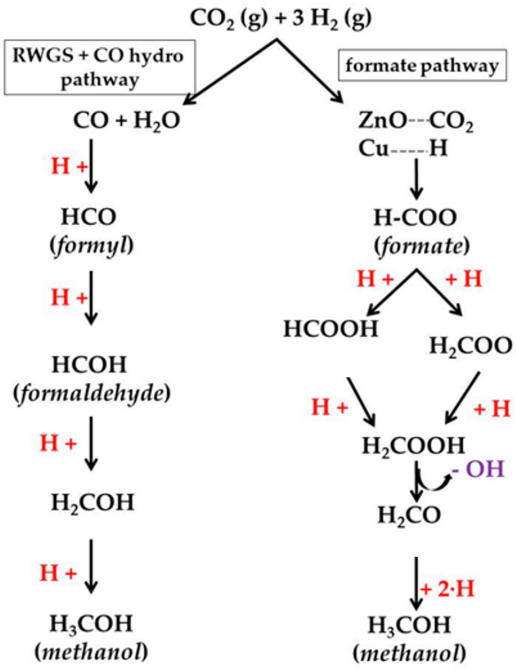

Scheme 1. Pathways of CH_3OH synthesis from CO_2 hydrogenation over Cu-based catalysts. Reproduced with permission from ref. [29] Copyright 2019 from MDPI under an open access Creative Commons CC BY 4.0 license.

designed for having an adequate pore dimension,[37] these active sites can be accessible to substrates and reagents. It has been frequently observed that the catalytic activity of MOFs in liquid phase reactions overcomes or is comparable with that of similar soluble metal complexes as homogeneous catalysts.[43] In many cases, it has been found that immobilization of the active sites in the lattice or encapsulation of the active site within the MOF pores is beneficial from the point of view of catalytic stability of the active centre, without introducing diffusion limitation to their accessibility.[44] In addition, the polarity environment of the MOF can also produce positive catalytic effects in comparison to homogeneous complexes.[45] In addition, MOFs exhibit well defined sites that can be tuneable in acid strength and electron density depending on the coordination with the ligand.[30,46] Figure 1 summarizes different opportunities to create active sites by appropriate selection of metal ions and linkers with or without functionalities.

Besides the use of MOFs with intrinsic catalytic activity, MOFs have also be used as supports.[48] MOFs have been widely used as porous host materials for the encapsulation of metal/metal oxide NPs, frequently observing that the activity of the resulting solids is often higher compared to the pristine NPs or NPs on other supports.[48–50] This higher activity is mainly due to the effective stabilization of metal NPs within the MOF by interaction of the NP guest with the linkers or the metal nodes present in the nanocavities offered by these solids. In addition, ligands can also be functionalized on purpose with carboxylate and amino groups as electron withdrawing and donating groups, respectively. In this way, besides direct interaction of these substituents with the surface of the metal NP, they can also influence the electronic density of the occluded metal clusters which in turn is expected to have control over the charge transfer between metal NPs and MOFs.[51]

In comparison to the massive use of MOFs as catalysts for liquid phase reactions, these solids have been used as gas phase catalysts in a limited number of cases.[47,52,53] The main obvious reason for this is the lack of thermal stability of these hybrid organic-inorganic materials.[54] Most frequently, due to the organic ligand, MOFs start to undergo structural collapse at temperatures around 250 °C and beyond this temperature also the organic ligand can undergo gradual decomposition.[54] While this general thermal instability of organic moieties is certainly a disadvantage in gas-phase reactions, there are examples of structurally highly robust MOFs that can stand temperatures of 350 °C without undergoing structural collapse or without significant ligand decomposition. In one of these examples, Daturi, Ferey, Serre and co-workers studied the thermal stability of MIL-

Amarajothi Dhakshinamoorthy received his Ph.D., degree in 2009 from Madurai Kamaraj University, Madurai-21, India. Later, he worked as a postdoctoral researcher with Prof. Hermenegildo Garcia at the Technical University of Valencia for four years. Currently, he is serving as UGC-Assistant Professor at School of Chemistry, Madurai Kamaraj University. His research interests include catalytic applications of metal–organic frameworks and graphene-related materials. He has co-authored over 185 publications, five book chapters and one patent. He is also serving as Early Carrier Advisory Board member in Molecular Catalysis, Elsevier.

Hermenegildo García is a full Professor at the Instituto de Tecnología Química of the Technical University of Valencia and Honorary Adjunct Professor at the Center of Excellence in Advanced Materials Research of King Abdullaziz University. He is working in the field of heterogeneous catalysis with porous solids as well as in the photocatalytic production of solar fuels having published over 900 articles. Prof. Garcia is Doctor Honoris Causa from the University of Bucharest, Spanish National Research award (2021), Janssen-Cilag award of the Spanish Royal Society of Chemistry (2011), Jaume I prize for Novel Technologies (2016) and Medal Lecturer award by the International Association for Advanced Materials (2021).

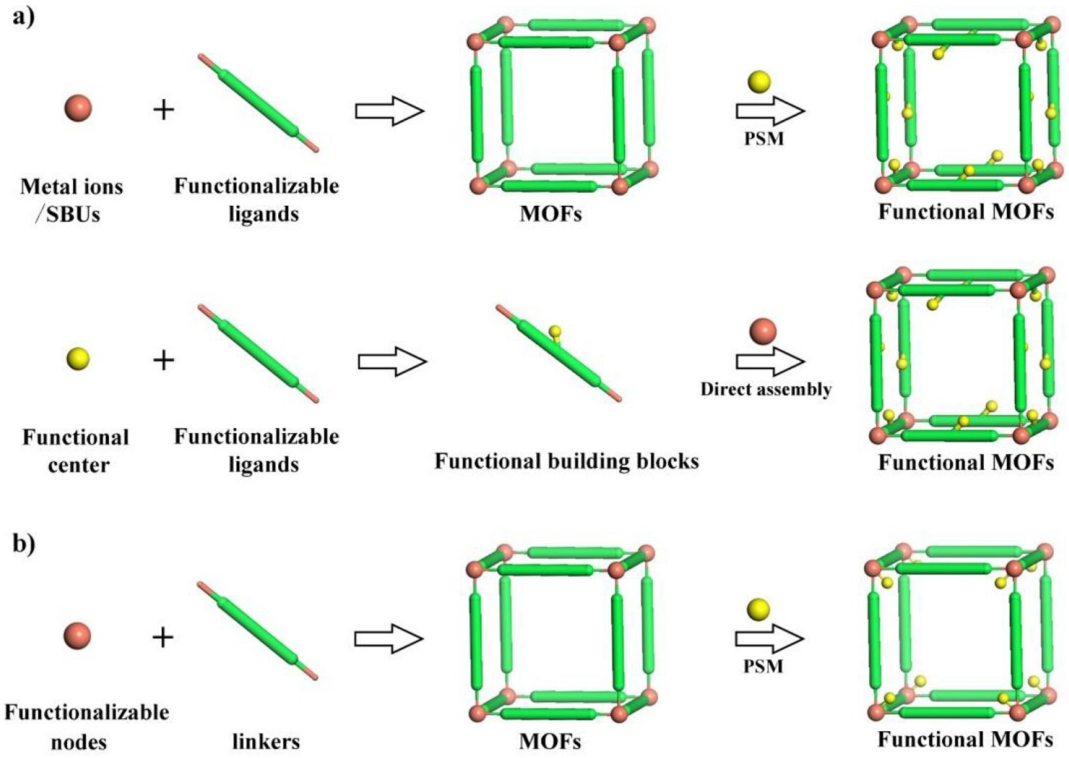

Figure 1. Illustration of the various possibilities to introduce and modify active sites on MOFs either at the linker (strategies a) or at the metal nodes (b). SBU: secondary building unit, PSM: post-synthetic modification. Reproduced with permission from ref. [47] Copyright 2019 American Chemical Society.

100(Fe) having trimeric Fe_3-μ_3O^{7+} nodes and 1,3,5-benzenetricarboxylate (BTC) as linker.[55] These studies established that at temperatures above 250 °C for 12 h, Fe(III) undergoes reduction to Fe(II), but this reduction was reversed upon cooling. MIL-100(Fe) was able to stand several heating at 250 °C and cooling cycles, decomposing at 280 °C.[56] Furthermore, the Cr-analogue [MIL-100(Cr)] does not undergo any change either in the oxidation state of the metal or ligand at 300 °C, decomposing at 327 °C.[57] In another example, Bordiga and Lillerud proved that UiO-66 having $Zr_6(\mu_3\text{-}OH)_4\mu_3\text{-}O_4^{12+}$ nodes and 1,4-benzenedicarboxylate (BDC) linkers can be heated at 400 °C without structural collapse. In the case of UiO-66, the structure undergoes thermal dehydration, but this change can be reversed upon cooling.[58] According to thermogravimetric analysis starting at 540 °C, UiO-66 lattice breakdown occurs with the rupture of the coordinative bond between the linker and the inorganic node and also the bond between the benzene rings and the terminal carboxyl group. In this way, the formation of benzene and CO_2 fragments are detected in the gas phase by mass spectroscopy.[59] However, since thermogravimetry is performed by increasing the temperature with time at a fixed rate, it could be that prolonged heating at temperatures lower than 540 °C could produce already a structural damage. In any case the thermal stability of UiO-66 is remarkable compared to other MOFs. There are other examples of remarkable stability as for instance the case of MIP-177(Ti)-HT or the ZIF-series showing that some particular MOFs can be used at temperatures above 300 °C without structural damage.[60]

Although gas phase reactions can be carried out at temperatures much higher than 400 °C in which most of MOF organic ligands will not survive, there is certainly a compatibility window between MOF thermal stability and suitable temperature of a gas phase reaction in which MOFs could be used as catalysts that would be worth to explore.[47,52] This is the case of CH_3OH synthesis from CO_2 hydrogenation. As it is indicated in Eq. 1, CO_2 hydrogenation to CH_3OH is one of the few exothermic reactions for CO_2. According to thermodynamics, this reaction should be carried out at low temperature, increasing the temperature being unfavourable for the CH_3OH proportion at the equilibrium. In fact, CO_2 hydrogenation to CH_3OH competes with CO_2 hydrogenation to CO (Eq. 2), corresponding to the RWGS reaction, that being an endothermic reaction is favoured by temperature increase. However, although thermodynamics indicate that low temperatures are preferable, kinetically the high energy barrier related to CO_2 activation makes necessary to increase the temperature to achieve any measurable reaction rate and CO_2 conversion. Most typically, CO_2 hydrogenation to CH_3OH is carried out at temperatures between 250 to 300 °C. Lower temperature than at 250 °C results in very low reaction rate and small CH_3OH production. Higher temperatures than 300 °C result in the prevalence of CO formation that kinetically is an easier reaction than CH_3OH formation. This temperature window between 250 and 300 °C could possibly allow the use

of certain MOFs as gas phase reaction catalysts, at least for the thermally most stable ones.

$$CO_2 + 3H_2 \rightleftharpoons CH_3OH + H_2O \quad \Delta G(25\,^{\circ}C) = -0.47\ kJ\ mol^{-1} \quad (1)$$

$$CO_2 + H_2 \rightleftharpoons CO + H_2O \quad \Delta G(25\,^{\circ}C) = 23.4\ kJ\ mol^{-1} \quad (2)$$

The present *minireview* wants to pay attention to the compatibility of various MOFs with CH_3OH synthesis from CO_2 and comment on the efforts already made to gain selectivity in this process. The importance of applying MOFs to CH_3OH synthesis derives from the consideration of two aspects. On one hand, in the new H_2 technology and targets for diminishing CO_2 emissions to the environment, CH_3OH could play a new role as liquid organic H_2 carrier and as energy vector. On the other hand, there is still not an ideal catalyst that is able to perform CO_2 hydrogenation with sufficient CH_3OH productivity, meaning high selectivity and high rate, therefore there being a need for the development of more advanced catalysts. Inspired by the activity of MOFs in liquid phase reactions, it can be easily anticipated that MOFs can also exhibit high efficiency for this reaction, provided that their structure does not collapse. It is the purpose of the present minireview to briefly describe the current state of the art on this specific, important, gas phase reaction and to provide some hints for further development of this area. Furthermore, MOFs have been used as sacrificial templates under thermal annealing under various atmosphere and conditions to produce the corresponding porous carbon-supported metal NPs, porous metal oxides, metal sulphides and other MOF derived materials. In these transformations, the organic linker is completely removed upon the treatment, resulting in active sites of different nature as those of the MOF. Thus, although MOF derived materials exhibit very interesting catalytic activity, these solids are beyond the scope of this minireview.

2. MOFs having intrinsic catalytic sites for selective CO_2 hydrogenation to CH_3OH

The most widely used industrial catalysts for CH_3OH synthesis from *syn gas* are based on supported mixed copper/zinc oxide materials, such as $Cu/ZnO/Al_2O_3$ (CuZnAl).[61] CuZnAl denotes a family of catalysts comprising Cu and ZnO NPs, with at least Cu/Zn mol ratio in the mixture of 1 or above. The spherical Cu NPs in the industrial catalyst are in close contact with ZnO NPs. Although the exact role of Cu and ZnO constituents is still debated, a large body of evidence confirms that ZnO dramatically increases the intrinsic activity of the copper catalyst, a phenomenon generally indicated as *Cu–ZnO synergy*.[62–64]

One of the simplest approaches to mimic this system in a MOF is to prepare a bimetallic Cu/Zn MOF in which the two metals are in the nodes. This approach was realized with ZnCu–MOF-74 that is a MOF with dipositive transition metal ions (Cu^{2+} and Zn^{2+}) and dihydroxyterephthalic acid as linker. It was expected that MOF-74 porosity will have significant influence on the facile accessibility of CO_2 and H_2 to nodal Zn and Cu metal sites uniformly located inside the ZnCu–MOF-74 channels. One of the syntheses for this bimetallic MOF-74 was ball milling solid-phase synthesis starting from the solid metal salts and organic precursors.[65] The control samples indicated that the monometallic Cu–MOF-74 is inactive for CO_2 hydrogenation reaction, however, ZnCu–MOF-74 affords moderate activity and selectivity towards CH_3OH. However, the activity and selectivity of CH_3OH of amorphous, mechanochemically desolvated ZnCu–MOF-74 was significantly increased compared to solvothermal synthesis of this material (Figure 2). In this way, the activity of crystalline ZnCu–MOF-74 sample was increased by 4–7 fold upon amorphization. The surface area of amorphous ZnCu–MOF-74 was about 250-times lower compared to its crystalline precursor which illustrates the role of defective sites as highly efficient catalytic centres for MeOH synthesis despite the low area of the amorphous ZnCu–MOF. Powder XRD of the sample used as catalyst indicated the formation of only traces of copper NPs in the amorphous matrix under reaction conditions. This study clearly proved the enhanced activity of the resulting amorphous solid, a fact that was attributed to the presence of defects and their beneficial influence on the catalytic activity. Isolated Cu atoms or small Cu clusters within the crystalline MOF favour the competitive RWGS reaction, while the amorphization tends to promote CH_3OH production. Therefore, the optimal ZnCu–MOF catalyst does not necessarily need to be the most crystalline sample, opening the door for the preparation of other MOF-like samples with the appropriate structure of the ZnCu centres, without necessarily pursuing the highest crystallinity.

Chen and co-workers have reported the importance of the ZnO/ZrO_2 interface with active Zr–Zn sites for CO_2 adsorption and observed formate intermediate on both Zn and Zr metal centres.[66] In another work, the existence of Zn in the ZrO_2 lattice in a Zr–O–Zn solid solution was supported by characterization data and based on isotopic H/D exchange experiments at 280 °C it was proposed that this Zr–O–Zn sites can adsorb H_2 and activate H–H bond splitting.[67] Furthermore, Zn–O–Zr sites in this solid solution can adsorb CO_2 as shown by temperature-programmed desorption of CO_2 and promote its conversion to CH_3OH. This type of Zn–O–Zr site is very easy to be mimicked on Zr MOFs with the advantage that the sites can be better defined, obtained in a high density, distributed uniformly in the solid and being accessible to reagents through the pores. In this context, Lin and co-workers have reported the formation of Zn^{2+}–O–Zr^{4+} sites in a Zr–MOF by post-synthetic treatment of $Zr_6(\mu_3\text{-}O)_4(\mu_3\text{-}OH)_4$ nodes of MOF-808 with $ZnEt_2$ to obtain MOF-808-Zn (Figure 3). MOF-808 contains $Zr_6(\mu_3\text{-}O)_4(\mu_3\text{-}OH)_4$ nodes, also present in UiO-66 and several other Zr–MOFs, and BTC as linker having a large specific surface area (about 1300 $m^2 g^{-1}$). The internal pores of MOF-808 have two types of cages with tetrahedral (4.8 Å diameter) and adamantane-like (1.8 Å diameter cavities) shapes. Note that both cages are accessible to CO_2 and H_2. Due to the association of Zn^{2+} to the

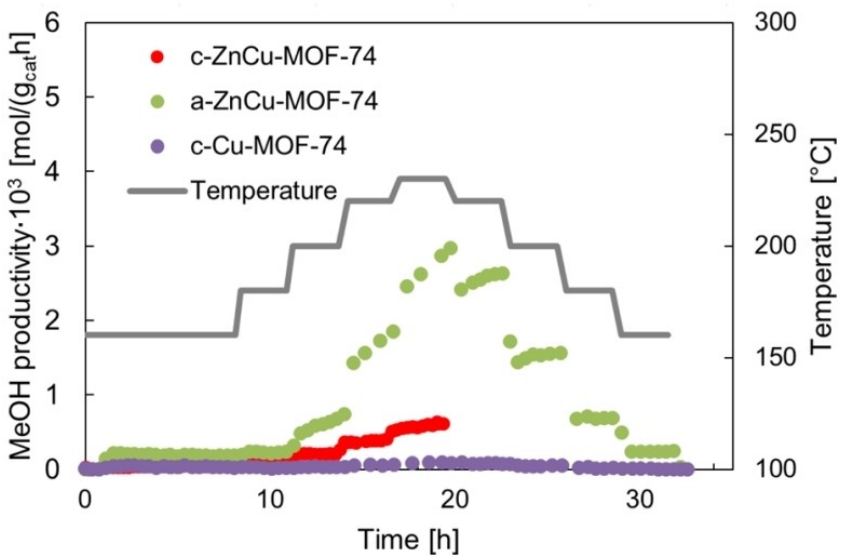

Figure 2. Evolution of MeOH molar productivity as a function of the reaction temperature during the catalytic experiments using related MOF-74 materials. Prefixes *"a-"* or *"c-"* means amorphous or crystalline, respectively. Reproduced with permission from ref. [65] Copyright 2021 American Chemical Society.

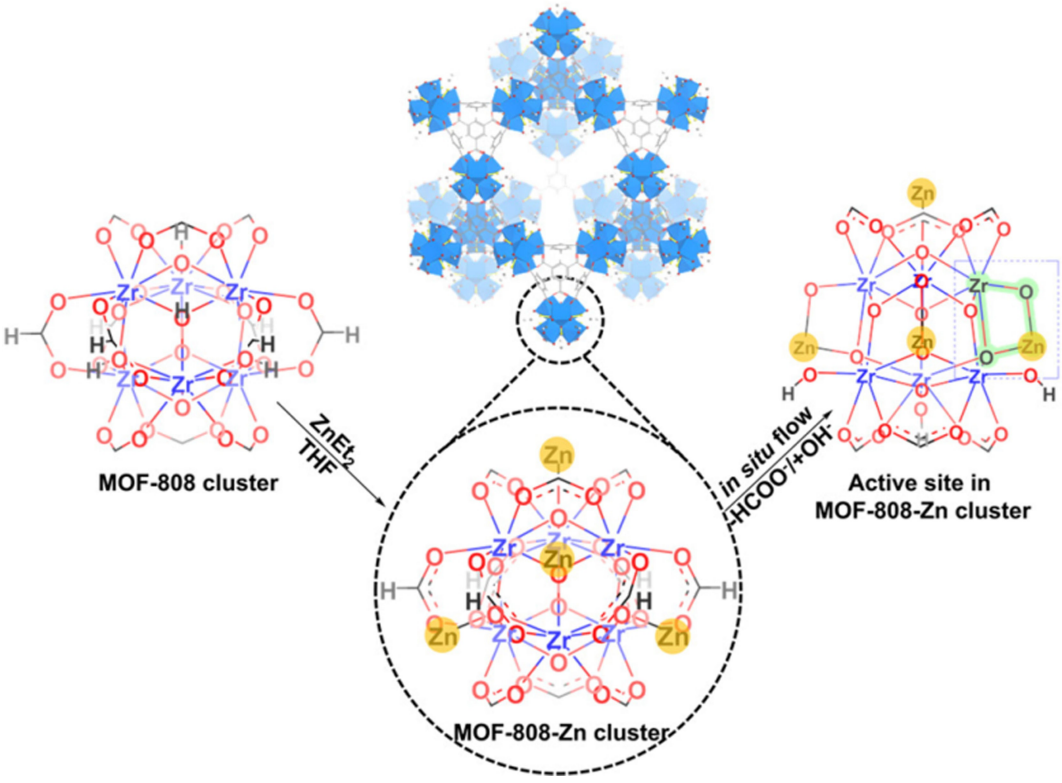

Figure 3. Synthesis of MOF-808-Zn and the structure of Zr^{4+}–O–Zn^{2+} sites proposed as responsible for selective CO_2 hydrogenation to CH_3OH. Reproduced with permission from ref. [68] Copyright 2021 American Chemical Society.

MOF nodes, this MOF catalyses CO_2 hydrogenation to CH_3OH.[68] MOF-808-Zn achieves >99% selectivity to CH_3OH in CO_2 hydrogenation with a high spatial time yield to CH_3OH (STY_{CH3OH}) of 190.7 $mg_{MeOH}\,g_{Zn}^{-1}\,h^{-1}$ at 250 °C. The catalytic activity was maintained for at least 100 h. X-ray absorption spectroscopy (XAS) indicated the presence of Zn^{2+}–O–Zr^{4+} sites and the absence of Zn_mO_n clusters. Temperature-programmed desorption measurements confirmed that H_2 activation occur at Zn^{2+} centres. Interestingly, Zn^{2+} sites attached to Zr-based nodes of other MOFs

without open Zr^{4+} sites failed to afford MeOH. The need for open Zr^{4+} sites in combination with the H_2 activating metal to enhance CH_3OH production was already demonstrated in other previous studies.[69–72] This work nicely characterized the role of well-defined Zn^{2+}–O–Zr^{4+} structures appended to metal-oxo nodes in MOFs to form an optimal catalytic site with the enhanced activity and selectivity to CH_3OH. It can be predicted that similarly to the Zn^{2+}–O–Zr^{4+} centres combinations of Zn^{2+} with other nodal metals, particularly those involving Cu, and even tri- or multimetallic sites could even result in an improved CO_2 activity with still high or complete CH_3OH selectivity. Theoretical calculations could shed light on the nature of these nodal metals. On the other hand, DFT calculations have clearly shown that Zn^{2+} is primarily responsible for H_2 activation and the Zr^{4+} site favours the adsorption of CO_2 and its conversion through the formation of formate as the reaction intermediate. The unique advantage of this solid is the well-defined local structure around the MOF lattice providing the opportunity for activation and adsorption through synergistic catalysis.

3. MOFs as porous supports of active guests

Due to the large pore volume, pore geometry with strictly regular dimensions, MOFs are also widely used as hosts to incorporate molecular guests and NPs with catalytic activity. These structural MOF properties suit particularly well for the preparation of supported metal and metal oxide NPs as catalysts for CO_2 hydrogenation. Supported metal NPs for CO_2 hydrogenation is an area that has received considerable attention,[66,73–77] with MOFs being still rarely used as hosts due to the thermal stability concerns as previously mentioned.

Continuing with the activity for MeOH production by the Zr–Zn couple of modified MOF-808,[68] the catalytic activity of ZnO–ZrO_2 mixed metal oxides,[78] ZnO–ZrO_2 aerogels,[79] and ZnO–ZrO_2 solid solutions have received some attention.[67] The superior performance of these solid catalysts is due to the *metal synergy* between Zn and Zr in ZnO or ZrO_2 supported solids, while catalysts without ZnO exhibited negligible activity.

In one of the recent reports using MOF as porous support for the Zn–Zr couple, ZnO NPs of 9 nm were incorporated within Zr-based MOF constructed by $Zr_{12}(\mu_3\text{-}O)_8(\mu_3\text{-}OH)_8(\mu_2\text{-}OH)_6$ clusters with biphenyldicarboxylate (bpdc) linkers and the activity of the resulting solid (ZnO/Zr_{12}-bpdc) was tested in the CO_2 hydrogenation to CH_3OH.[80] As shown in Figure 4, $ZnEt_2$ was coordinated to μ_3-O atoms of the metal cluster forming ZnEt–O–Zr_{12}-bpdc, which was subsequently oxidized to ZnO NPs to form ZnO/Zr_{12}-bpdc catalyst. ZnO/Zr_{12}-bpdc catalyst exhibited a CO_2 conversion of 7.5 % with a STY of 110 $mg_{MeOH}\,g_{catalyst}^{-1}\,h^{-1}$ or 440 $mg_{MeOH}\,g_{Zn}^{-1}\,h^{-1}$ with >95 % selectivity to CH_3OH at 250 °C. No evidence of ZnO particle growth was observed after 100 h of reaction at 250 °C. As an important data hinting for future directions in the field, the activity of ZnO/Zr_{12}-bpdc was further enhanced by Co doping (ZnO/Zr_{12}-bpydc-$Co(NO_3)_2$), reaching a STY of 219 $mg_{MeOH}\,g_{catalyst}^{-1}\,h^{-1}$ at 16 % CO_2 conversion under similar conditions. This enhanced activity of ZnO/Zr_{12}-bpydc-$Co(NO_3)_2$ is attributed to the synergistic effect derived from the presence of three metals. Obviously, the possible combinations of three or more metals and determination of their optimal proportions opens a vast chemical space with a high potential for leading to an increase in the catalytic activity for CH_3OH production. It is, however, worth to comment that linkers of long dimensions, such as bpdc, result generally in MOFs of lower thermal stability, due to the large pore dimensions of these materials. Considering the dimensions of reagent (CO_2 and H_2) and product (CH_3OH) it appears that no large pore size is not necessary to perform the reaction. Control experiments indicated that Zr_{12}-bpy-Co preferentially converts CO_2 to HCOO* while the Zn–Zr site favours the hydrogenation of HCOO* to CH_3OH. Thus, this work nicely illustrates the assembly of Zr_{12}-bpy-Co site and the Zn–Zr sites as complementary targeting for steps in the hydrogenation of CO_2.

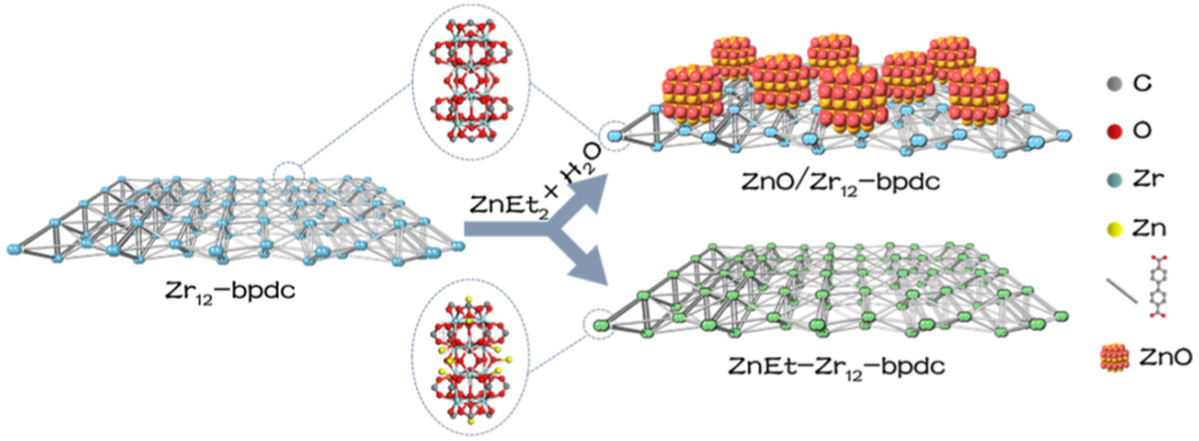

Figure 4. Preparation of well-defined ZnO–Zr catalysts via post-synthetic metalation of Zr_{12}-bpdc MOF and subsequent oxidation. Reproduced with permission from ref. [80] Copyright 2021 American Chemical Society.

As it has been sufficiently stressed, one of the main problems of MOFs for gas phase reactions is the lack of thermal stability, illustrated in the previously commented case of MOF-74. One original way to overcome this drawback that has been proposed is the post-synthetic treatment of a MOF by incorporating siliceous linkers. The resulting so-called *Si-infused* UiO-66 (s-UiO-66, Figure 5) still exhibits well-developed porosity but in addition a significant thermal and structural stability.[81] This sample, s-UiO-66 containing silicone linkers was used as a host to confine homogeneously dispersed ultrafine CuO NPs (CuO/s-UiO-66) that should act as active sites. Selective hydrogenation of CO_2 to CH_3OH using CuO/s-UiO-66 as catalyst exhibited STY_{CH3OH} of 2649 $mg\,g_{Cu}^{-1}\,h^{-1}$ which is significantly higher than to Cu/ZrO_2-based (159 $g_{MeOH}\,kg_{cat}^{-1}\,h^{-1}$) catalysts (Figure 6).[81] Interestingly, the activity of CuO/s-UiO-66 catalyst (4.35 wt % Cu) was about two-fold higher than to commercial $Cu/ZnO/Al_2O_3$ catalyst at 240 °C under the same reaction conditions. This enhanced activity of CuO/s-UiO-66 is proposed to derive from its robust structure at the reaction temperature, preventing the agglomeration of CuO NPs. Characterization of spent catalyst reveals that no sintering of Cu NPs or appearance of a ZrO_2 phase occurs after 130 h of time on stream. Moreover, in situ characterizations indicate that a key factor in the activation of H_2 is the generation of metallic Cu NPs, while s-UiO-66 matrix contributes adsorbing CO_2 in the form of carbonate species. Furthermore, detailed in situ DRIFTS spectra measurements have revealed that Cu^0 is identified to be responsible for the activation of H_2 while s-UiO-66 adsorbed CO_2 in the form of carbonate species. Later, these adsorbed species are subsequently reduced with the assistance of activated H_2 leading to the formation of carbonyl and formate intermediates, which were later hydrogenated to CH_3OH.

CuO NPs have also been incorporated in Zr/Hf-based MOFs and their activity has been compared with that of other supports for CO_2 hydrogenation to CH_3OH.[82] The series of catalysts that were compared in the study includes $Cu/\gamma\text{-}Al_2O_3$, Cu/ZIF-8, Cu/MIL-100 and Cu/UiO-66.[82] Catalytic measurements showed that UiO-66 as support results in the highest activity. For instance, Cu/UiO-66 showed a production of CH_3OH 70 times higher than to $Cu/\gamma\text{-}Al_2O_3$ under identical conditions. Interestingly, the replacement of Zr^{4+} by Hf^{4+} in UiO-66 tripled the formation rate of CH_3OH (Figure 7). Furthermore, Cu/UiO-66-COOH afforded a three-fold enhancement in the production of CH_3OH compared to UiO-66 or UiO-66-NH_2. These catalytic data firmly indicate that it is possible to enhance the catalytic activity of the incarcerated Cu NPs by modulating the interaction of the MOF structure with the incorporated Cu NPs and this can be achieved by selecting the nature of the metal at the nodes and by substituents on the linker. Apparently, the MOF linkers interact with the surface of the metal oxide NPs modulating the electron density at the Cu sites. While this is well known in molecular complexes and the ligand effect in colloidal metal NPs is also known, this tool remains mostly unexplored in catalysis by metal NPs within MOFs and can result in unforeseen results. The

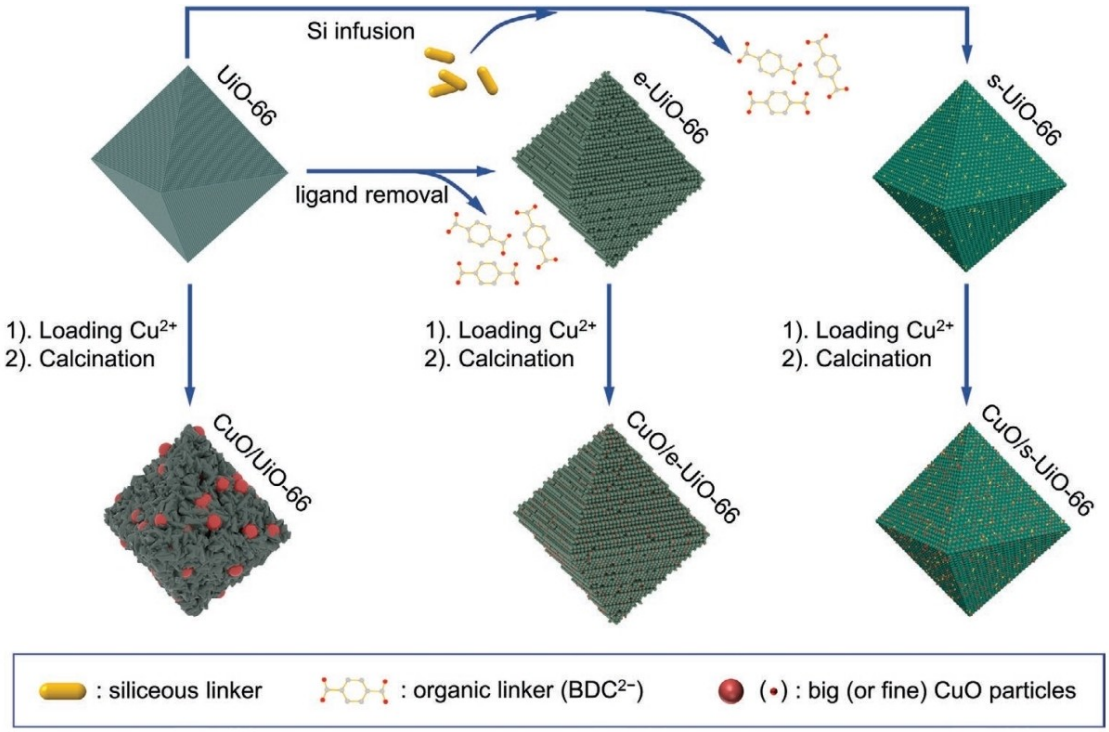

Figure 5. Schematic illustration of three post-synthetic modifications of UiO-66 to obtain Cu containing material either loading Cu^{2+} followed by calcination or etching ligands with or without Si infusion Cu catalysts (BDC^{2-}: 1,4-benzenedicarboxylate anions; e-UiO-66: etched UiO-66; s-UiO-66: Si-infused UiO-66; siliceous linker: oligomeric siliceous species). Reproduced with permission from ref. [81] Copyright 2023 Wiley.

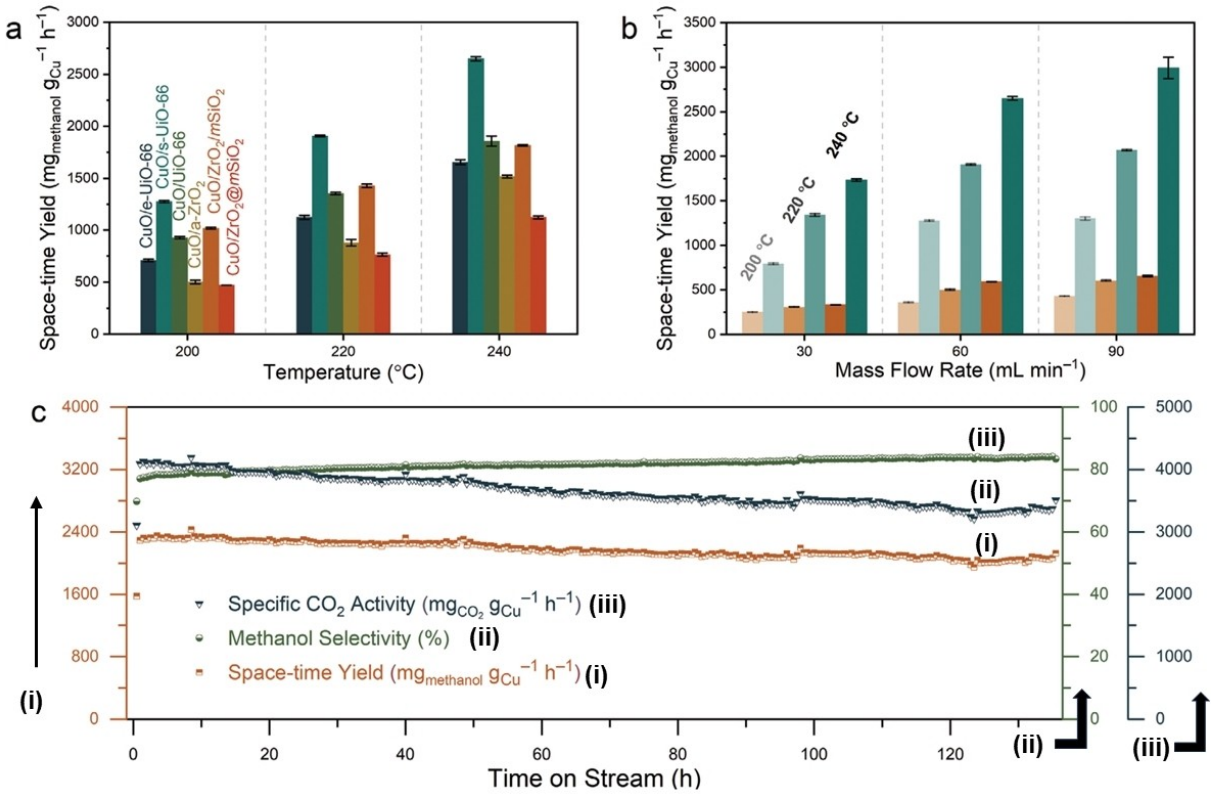

Figure 6. a) Comparison of the catalytic performance at three different temperatures of CuO/UiO-66, CuO/e-UiO-66, CuO/a-ZrO_2, CuO/ZrO_2/$mSiO_2$, CuO/ZrO_2@$mSiO_2$, and CuO/s-UiO-66 at a weight hourly space velocity of 18000 mL $g_{catalyst}^{-1}$ h^{-1} (see color codes for each sample) b) STY_{CH3OH} of CuO/s-UiO-66 (4.35 wt% of Cu) (green) and commercial Cu/ZnO/Al_2O_3 (orange) at different mass flow rates and temperatures. c) Stability test of CuO/s-UiO-66 (4.29 wt% of Cu) at 240 °C and 18000 mL $g_{catalyst}^{-1}$ h^{-1}. See Roman numerals in the plots corresponding to the same numerals in the y-axis scale. Reaction pressure is 3.0 MPa. Reproduced with permission from ref. [81] Copyright 2023 Wiley.

reason is that the number of groups (carboxylic acid and carboxylate in the case of Cu/UiO-66-COOH) surrounding the Cu NPs can be controlled and this number is countable and located at precise geometrical positions. Since ligands generally decrease the catalytic activity in colloidal NPs by blocking or competing with the active sites, the fact that in MOF cavities there are only 12 carboxylic groups, and that even this number can be further diminished and optimized in mixed ligand MOFs, gives the opportunity to have a high control on the electron density and of the NP surface with these ligands, as illustrated here, for the case of Cu NP. It would have been interesting to combine the two parameters (Hf and COOH groups of the linker) in a single MOF material to reach the highest possible CH_3OH production enhancement. Although authors claim that the rate-determining step for the conversion of CO_2 to CH_3OH is hydrogenation of formate, no experimental data to explain the mechanism were provided.

MnOx/mesoporous Co_3O_4 catalyst was reported as an efficient solid catalyst to produce CH_3OH by hydrogenation of CO_2 at mild temperature (250 °C) and pressures (6 bar).[83] Although MnOx/mesoporous Co_3O_4 exhibited high activity, CH_3OH selectivity was moderate due to the formation of other products like hydrocarbons and/or CO and, a further improvement would be to increase this CH_3OH selectivity without affecting negatively to the activity. Thus, in a study to use MOFs to enhance and gain control on the activity of Cu NPs in CO_2 hydrogenation, individual Cu nanocrystals (NCs) were surrounded by the framework of UiO-66 and the activity of the resulting Cu(core)⊂UiO-66(shell) solid was tested in the hydrogenation of CO_2 to CH_3OH.[69] The size of Cu NC was 18 nm and it was at the centre of the UiO-66 shell about 100 nm (Figure 8). The catalytic activity of Cu⊂UiO-66, was compared with that of Cu on UiO-66 (external surface), Cu on ZrO_2, and Cu/ZnO/Al_2O_3 for CO_2 to CH_3OH reaching the TOF values of 3.7×10^{-3}, 1.7×10^{-3}, 0.42×10^{-3}, and 0.45×10^{-3} s^{-1}, respectively at 175 °C and 10 bar using CO_2 and H_2 in a 1:3 molar ratio. In contrast, no activity was observed with Cu NCs on MIL-101(Cr) and Cu NCs⊂ZIF-8 under similar conditions. Furthermore, Cu⊂UiO-66 afforded 8-fold higher yield with 100% selectivity to CH_3OH compared to the benchmark Cu/ZnO/Al_2O_3 catalyst. XPS analysis of Cu⊂UiO-66 revealed that Zr 3d binding energy is shifted to lower oxidation state when UiO-66 embeds Cu NC, suggesting the presence of a strong interaction between Cu NC and Zr oxide in the MOF, thus, explaining the very high activity of the core–shell system. Authors have postulated that metallic Cu species are responsible for the activation of H_2 and formate intermediates are stabilized by

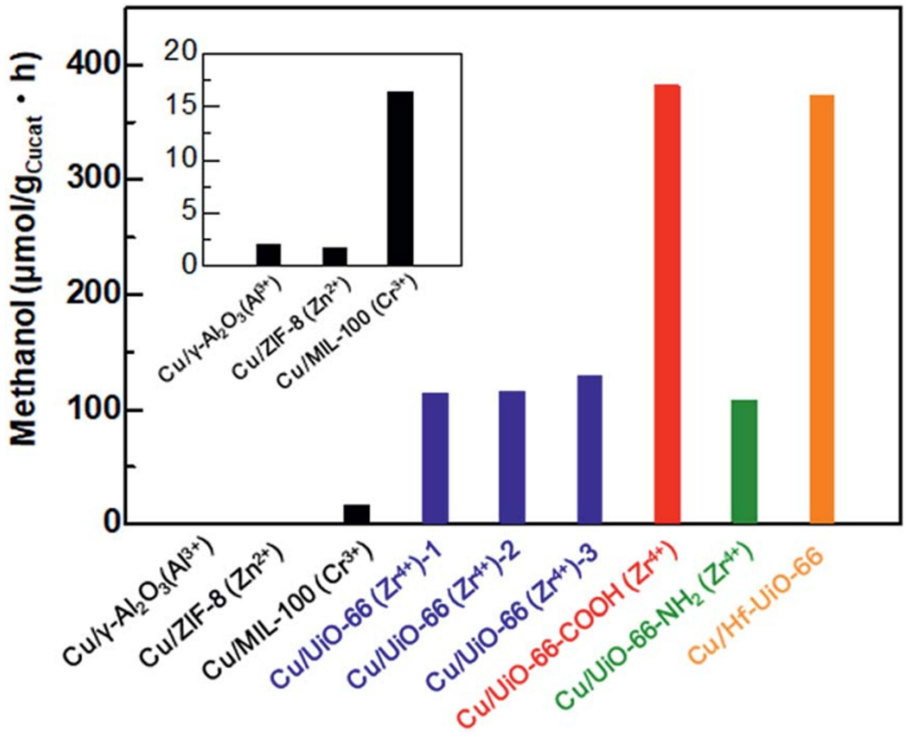

Figure 7. STY of CH_3OH synthesized from CO_2 and H_2 using Cu/γ-Al_2O_3 and various Cu/MOF composites catalysts. The number of defects was estimated from the discrepancy of the ideal formula $Zr_6O_4(OH)_4(BDC)_6$ with the empirical for $[Zr_6O_4(OH)_4(BDC)_{5.7}]$, $[Zr_6O_4(OH)_4(BDC)_4.5(AcO)_3]$ and $[Zr_6O_4(OH)_4(BDC)_3.6(AcO)_{4.8}]$ for Zr–UiO-66-1, Zr–UiO-66-2 and Zr–UiO-66-3, respectively. AcO: acetate. Reproduced with permission from ref. [82] Copyright 2019 Royal Society of Chemistry under Creative Commons Attribution 3.0 Licence.

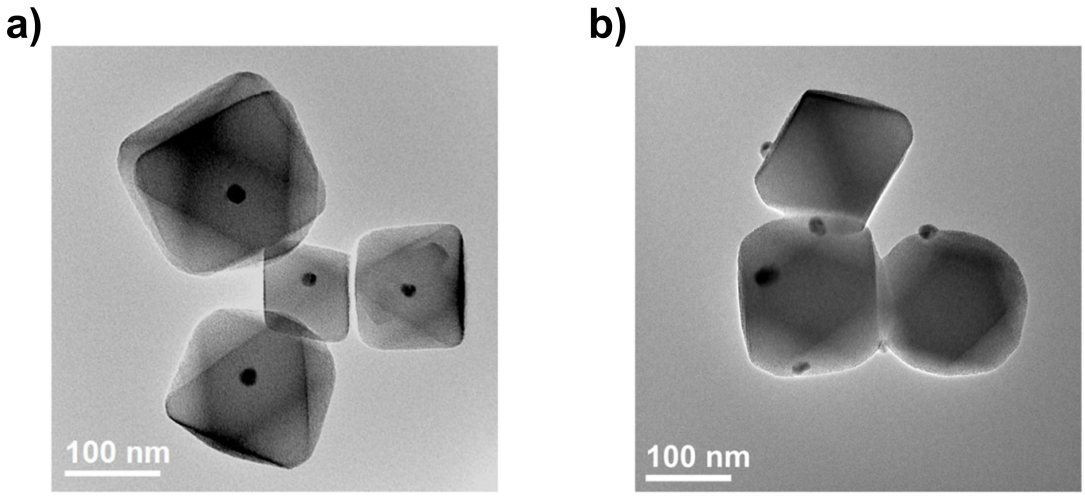

Figure 8. TEM images of (a) Cu⊂UiO-66 (single Cu NC inside UiO-66 of well defined octahedral morphology), (b) Cu on UiO-66. Reproduced with permission from ref. [69] Copyright 2016 American Chemical Society.

cationic Cu species. However, no spectroscopic data to support these conclusions were provided.

In other study, Cu NPs were deposited over UiO-66 MOFs at two different levels of Cu exchange to obtain Cu/UiO-66-a (43.2 % OH exchange by Cu) and Cu/UiO-66-b (18.3 %) (Figure 9) and the activity of these two solids was examined in the CO_2 hydrogenation to CH_3OH.[70] Cu/UiO-66-a exhibited a remarkable rate of CH_3OH production to 4.7 $mol_{CH3OH}\,mol_{Cu}^{-1}\,h^{-1}$ at 250 °C at 32 bar pressure. This production rate was almost an order of magnitude higher compared to benchmark catalysts, Cu/ZrO_2 and $Cu/ZnO/Al_2O_3$, and almost two orders of magnitude higher than to Cu/UiO-66-b. This significant difference in the activity among these catalysts was ascribed to the specific anchoring of Cu NPs to the support. On the other hand, Cu/UiO-66-a afforded 29 % selectivity to CH_3OH compared to 7 % with

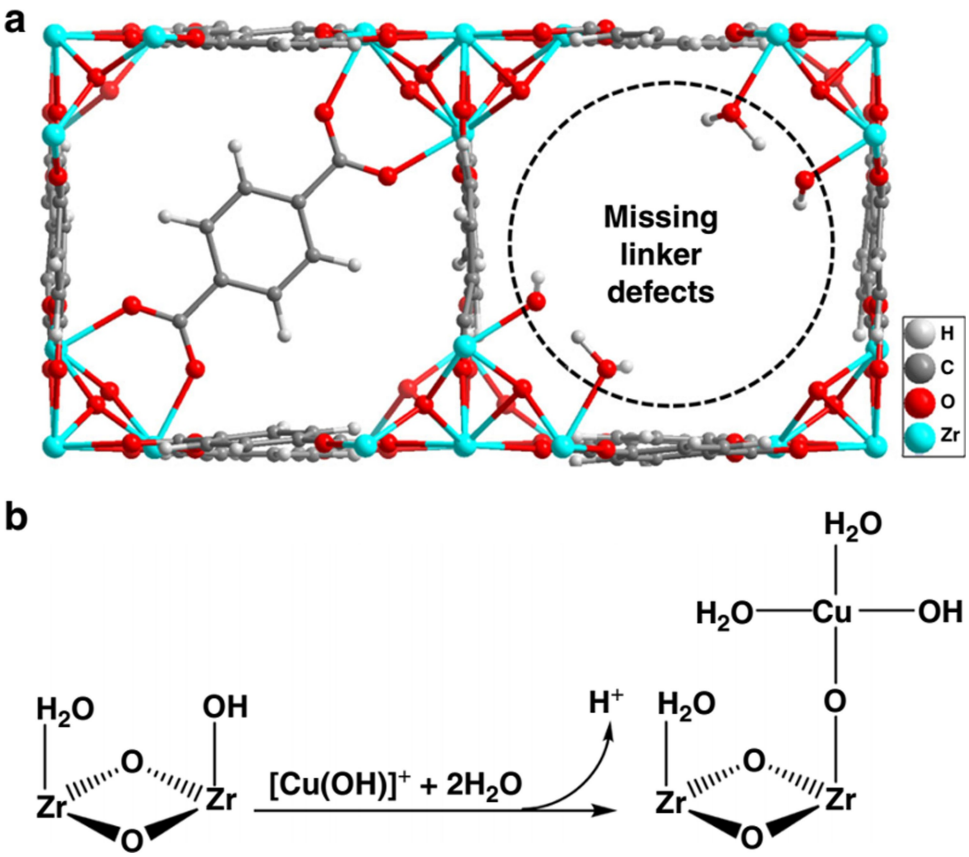

Figure 9. (a) Illustration showing a missing linker in the UiO-66 structure being replaced by two –OH/OH_2 groups, which are specific sites for ion exchange to anchor metal ions, such as Cu^{2+}, onto the Zr_6 nodes of the MOF; (b) Proposed reaction for Cu anchoring (H^+ exchange) in aqueous solution and plausible structure of the resulting site with activity in CO_2 hydrogenation to CH_3OH. Reproduced with permission from ref. [70] Copyright 2020 Nature Portfolio under a Creative Commons Attribution 4.0 International License.

$Cu/ZnO/Al_2O_3$. The superior performance of Cu/UiO-66-a derives from the small size of metallic Cu NPs and the high population of Cu–O–Zr interfacial sites that were proposed as responsible for selective CH_3OH synthesis. Interestingly, the production rate of CH_3OH with Cu/UiO-66-a was stable for 50 h on stream, suggesting that the MOF can stand these conditions. Furthermore, XANES measurements of the fresh and the spent Cu/UiO-66-a were identical, thus showing the notable structural stability under reaction conditions, even without change in the proportions between metallic and cationic Cu. Efforts to identify the reaction intermediates for the conversion of CO_2 to CH_3OH by in situ IR study failed to detect any species.

Cu NPs and Cu–ZnO nanocomposites have been incorporated into amorphous UiO-66 (amUiO-66) to obtain Cu/amUiO-66 and Cu–ZnO/amUiO-66 (Figure 10). These samples were prepared by spray-drying method in which DMF droplets containing seeds of UiO-66 and salts of Cu with or without Zn salts are quickly evaporated.[84] Under these conditions, immediate formation of amUiO-66 containing the metal NPs occurs. amUiO-66 synthesised in this way has high porosity, but lacks the long-range order expected for crystalline UiO-66 samples and responsible for the characteristic XRD patterns. am-UiO-66 solids were characterized by HRTEM, EDX, powder XRD and EXAFS to gain information on the structure of the nanocomposites and MOF. It can be concluded that amUiO-66 was essentially the same structure and coordination bonds as of UiO-66. The performance of Cu/amUiO-66 for CO_2 hydrogenation to CH_3OH was 3-fold higher compared to Cu/crystalline UiO-66.[84] Furthermore, Cu–ZnO/amUiO-66 reached STY for MeOH production of 710.5 $\mu mol\, g_{Cu}^{-1}\, h^{-1}$, surpassing by a factor of 1.5-fold to the performance of Cu/amUiO-66 and 2.5-fold to the productivity value for $Cu–ZnO/\gamma\text{-}Al_2O_3$ (Figure 10). In situ FT-IR spectroscopy and XPS measurements were performed to characterize the nature of support and understand its high activity. The results from these analyses indicate that Cu NPs stabilized in Cu/amUiO-66 and Cu–ZnO/amUiO-66 are distributed uniformly within the pores and the relatively few defects of amUiO-66 favour the stabilization of zero valent Cu as small clusters or single atoms respect to Cu NPs in crystalline UiO-66 and $Cu–ZnO/\gamma\text{-}Al_2O_3$. In addition, amUiO-66 is also believed to play an important role promoting the dissociation of H_2 and its spillover to low coordinated Zr sites in Cu/amUiO-66 and Cu–ZnO/amUiO-66 increasing the conversion of CO_2 to CH_3OH. This study nicely illustrates the possible positive role that defects can play to increase the catalytic activity in MOF supported Cu NPs. The two main bottlenecks that still would be important to overcome are

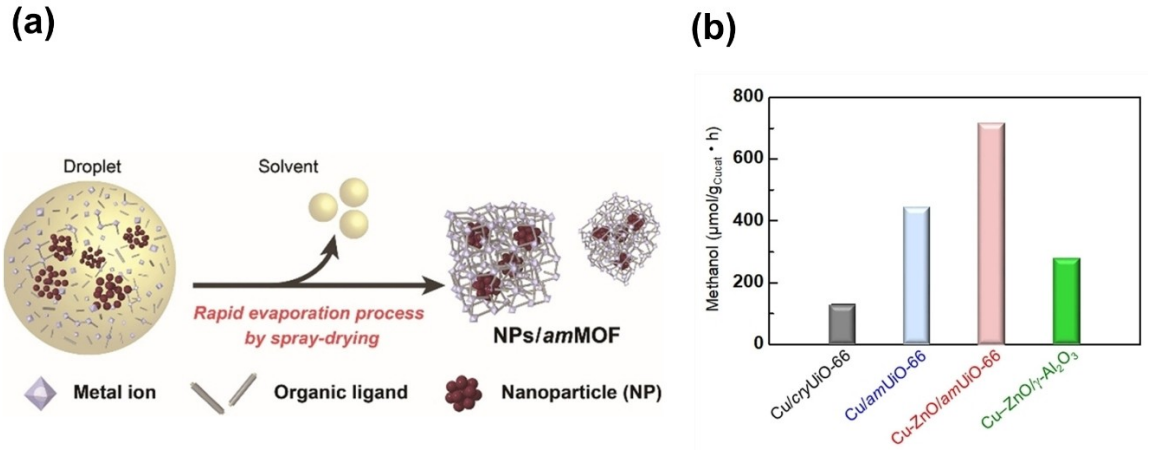

Figure 10. (a) Cu/amUiO-66 and Cu–ZnO/amUiO-66 synthesized by the spray-drying method; (b) Amount of CH_3OH produced from CO_2 and H_2 by Cu NPs in crystalline UiO-66 (Cu/cryUiO-66), Cu/amUiO-66, Cu–ZnO/γ-Al_2O_3, and Cu–ZnO/amUiO-66 catalysts. Reproduced with permission from ref. [84] Copyright 2021 Wiley.

the low specific surface area (190 vs. 702 $m^2 g^{-1}$ for Cu/am-UiO-66 in comparison to crystalline UiO-66) and the relatively large size of the metal NPs formed (25.1 ± 5.0 for Cu/am-UiO-66 in comparison to 13.1 ± 3.9 nm on crystalline UiO-66). Optimization of these two important factors is, certainly, a reasonable direction to further improve the activity of these amorphous MOFs as selective catalysts. Efforts to identify the reaction intermediates in the conversion of CO_2 to CH_3OH with this catalyst would certainly assist a better understanding the reaction process.

ZrO_2 has been reported as an effective support to promote the dispersion and reaction stability of CuO–ZnO NPs, thus making CuO–ZnO/ZrO_2 solids as one of the state-of-the-art Cu-based catalysts in the CO_2 hydrogenation to CH_3OH.[85,86] Unfortunately, Cu NPs on CuO–ZnO/ZrO_2 catalyst tend to aggregate gradually at the reaction temperatures normally used in CO_2 hydrogenation, resulting in a decrease in the population of active Cu/ZnO_x interfaces along the time on stream. On other hand, separated Cu particles lacking Zn are more prone to promote the RWGS reaction resulting in lower selectivity of CH_3OH. Therefore, one of the key roles of the support should be to increase the stability of Cu–ZnO_x particle size and maintain Cu–Zn interfaces by establishing strong metal-support interactions that should result in an improved catalyst performance. In a new strategy for the construction of stable CuO–ZnO/ZrO_2 catalyst, UiO-66 was used as support for the encapsulation of a series of Cu–Zn catalysts with various metal loadings by employing the deposition-precipitation method.[87] The catalytic activity of Cu–Zn@UiO-66 solids was tested in the hydrogenation of CO_2 to CH_3OH. Among the various solids prepared and tested for this reaction, the highest activity was achieved with Cu–Zn@UiO-66 catalyst with Cu–Zn loading of 35 wt % (Cu/Zn mol ratio: 2.5) that exhibited 9.1 % yield of CH_3OH with 18.5 % CO_2 conversion (STY_{CH3OH} of 2.4 $mmol_{CH3OH}\, g_{cat}^{-1}\, h^{-1}$) at 240 °C (Figure 11). Under these conditions, the catalyst was stable for 100 h. This superior activity was ascribed to the ultra-small Cu–Zn NPs (4 nm), high density of Cu/ZnO_x interfaces confined within UiO-66 framework and the strong interaction between Cu and ZnO_x.

Mesoporous zeolites have also been reported to prevent agglomeration of metal NPs by confining them in their nanochannels.[88–90] In view of these precedents and considering that zirconia is a good support of Cu NPs, not surprisingly, porous MOFs can combine both the confinement effect within the pores and the strong metal-support interactions with Zr-metal oxo clusters and metal-coordinating sites at ligands to develop suitable supports for Cu-based CO_2 hydrogenation catalysts. As a realization of this idea, Lin and co-workers have reported the combination between 2,2′-bipyridyl (bpy) and $Zr_6(\mu_3\text{-}O)_4(\mu_3\text{-}OH)_4$ clusters to form UiO-bpy able to stabilize ultra small Cu/ZnO_x NPs (1 nm) encapsulated within the voids, avoiding their agglomeration (Figure 12). Bipyridyl should play the role of internal ligands around the Cu/ZnO NPs incorporated within the pores. The MOF cavities provide also well-defined compartmentalization of Cu and ZnO_x for which confinement effect can apply.[91] At 250 °C and 4 MPa with a H_2/CO_2 ratio of 3, the activity of Cu/ZnO_x@UiO-bpy catalyst exhibited a STY up to 2.59 $mg_{MeOH}\, g_{Cu}^{-1}\, h^{-1}$ with complete selectivity to CH_3OH. Besides, the catalyst was also stable for 100 h. The high activity of this solid was attributed to the strong metal-support interaction between NPs and the organic chelates and the metal-oxo clusters. These results clearly encourage for the development of related catalysts taking advantage of the availability of a wide range of MOFs with different linkers able to act as ligands of Cu and ZnO_x and oxo metal clusters interacting with them, but enjoying higher thermal stability that could allow to perform the reaction to somewhat higher temperature. Authors believe that H_2 is homolytically dissociated on the Cu surface by forming Cu–H species. The dissociated H_2 spillovers to Zr sites present on the SBUs and defect sites on ZnOx. Also, CO_2 is adsorbed on unsaturated Zr sites and ZnOx by forming carbonates and bicarbonates, which are rapidly hydrogen-

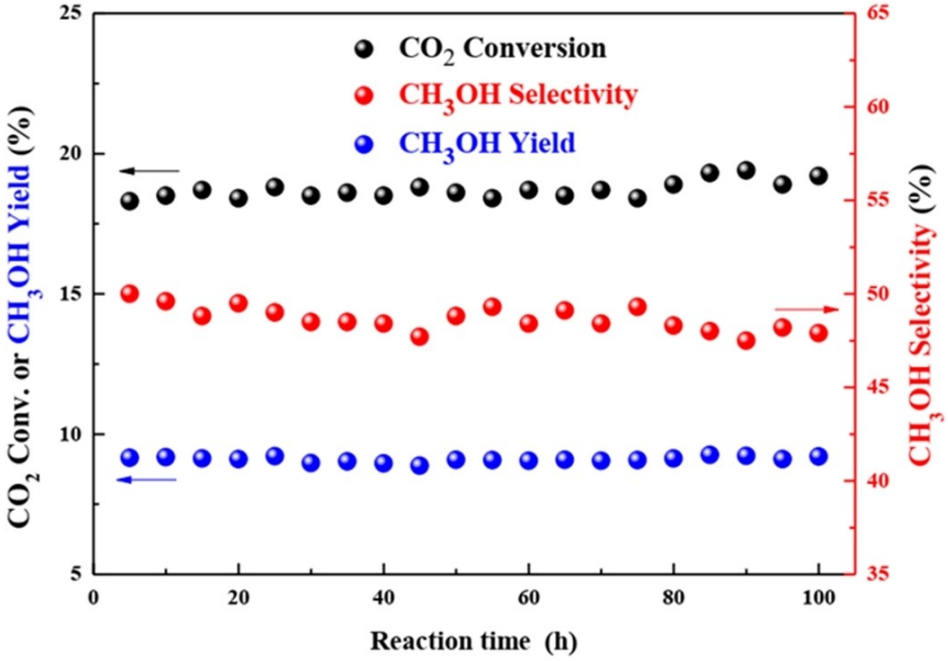

Figure 11. Catalytic performance vs. time-on-stream for the 35 wt% Cu–Zn@UiO-66 (T = 240 °C, P = 3.0 MPa, H_2/CO_2: 3, GHSV = 2400 h^{-1}). Reproduced with permission from ref. [87] Copyright 2022 Elsevier.

ated from spillover. Meanwhile, H_2 spillover also reduces some Zr(IV) to Zr(III) and some Zn(II) to Zn(0) as shown by XPS. The synergistic processes like H_2 activation on Cu and CO_2 activation on ZnOx and Zr SBUs sites favour to achieve superior activity by the catalyst. This proposal is shown in Figure 13.

In another study, Pt NPs (average size 3.6 ± 0.7 nm) were embedded within the framework of UiO-67 and the activity of Pt@UiO-67 sample was tested in the hydrogenation of CO_2 to CH_3OH at 170 °C and 1–8 bar pressure.[71] CH_3OH selectivity increased from 3 to 19 % (TOF: 0.01 s^{-1}) when the pressure raised from 1 to 8 bar, with only a slight increase in methane selectivity from 1.2 to 1.6 %. In comparison, Pt/Al_2O_3 showed the formation of methane and CH_3OH, with CH_3OH selectivity reaching 10 % at 8 bar pressure. In contrast to Pt@UiO-67, methane selectivity in Pt/Al_2O_3 increased substantially with increasing pressure. For Pt/SiO_2 and Pt/C as catalysts, CO was the only product detected. The available evidence suggests that CH_3OH is formed as consequence of the possible influence of the interface between Pt NPs and defective Zr nodes favouring the formation of formate intermediates attached to the Zr nodes.

Later, the same group has extended their work by studying the dynamic role of the Zr-node in Pt@UiO-67 and the influence of H_2O on the CO_2 hydrogenation at 170 °C.[72] This work has shown that an increasing number of Zr-node defects enhances the formation of both CH_3OH and methane. In addition, CO_2 hydrogenation on prehydrated Zr-nodes exhibited higher initial CH_3OH and methane formation rates than dehydrated Zr-node. Experimental evidence by transient kinetics suggest that these results are due to the competitive adsorption between CH_3OH and water.

The composition of the metal nodes of UiO-66 can be tuned by introducing other metals besides Zr^{4+}. In this way, Cu^{2+} ions have been supported on UiO-66(Zr) and UiO-66(Ce/Zr), testing their activity in the hydrogenation of CO_2 to CH_3OH.[92] The results indicated a significant increase in CH_3OH selectivity for bimetallic UiO-66(Ce/Zr) compared to monometallic UiO-66(Zr), but without increasing in the CH_3OH production rate (Figure 14). This study experimentally showed that the selectivity of CH_3OH can be influenced by the nodal composition of UiO-66, opening the way for an optimization of the CH_3OH selectivity by selecting the appropriate metal on the node. However, the situation is much more complex when H_2 activating metal such as Cu is already present in the structure. In this way, as shown in Figure 14, due to the presence of Cu, selectivity to CH_3OH even decreases slightly in Cu/UiO-66(Ce/Zr) compared to monometallic Cu/UiO-66(Zr) and CH_3OH productivity significantly decreases for the bimetallic Cu/UiO-66(Ce/Zr). Computational calculations should clarify the interplay between nodal metal ions and CH_3OH selectivity and productivity and should lead the experimental work by providing the most suitable combination of metal nodes to enhance CH_3OH production.

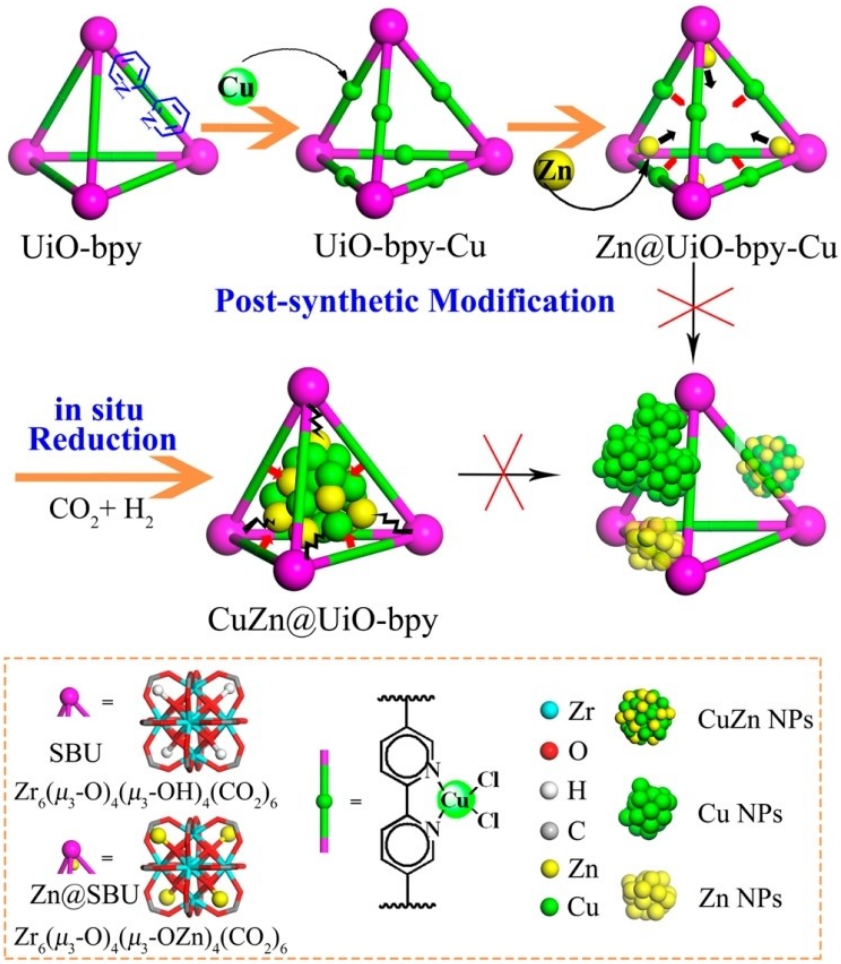

Figure 12. Preparation of CuZn@UiO-bpy via in situ reduction of post-synthetically metalated UiO-bpy. Reproduced with permission from ref. [91] Copyright 2017 American Chemical Society.

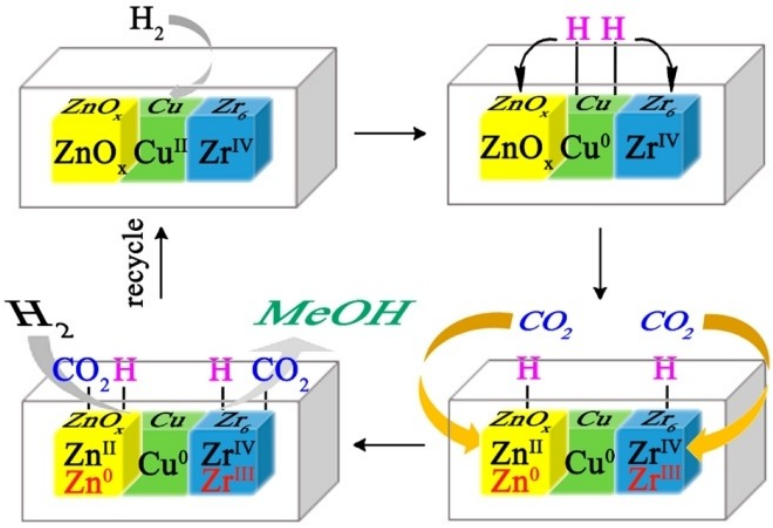

Figure 13. Encapsulated active sites in MOFs and their functions in catalytic CO_2 hydrogenation. Reproduced with permission from ref. [91] Copyright 2017 American Chemical Society.

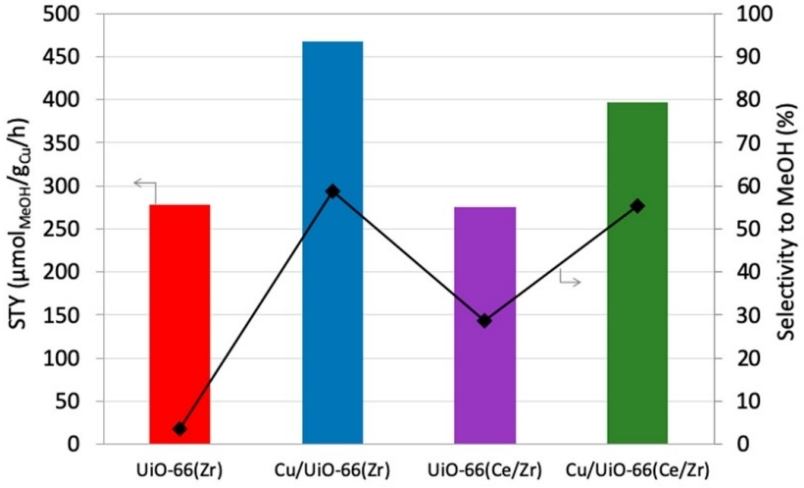

Figure 14. Selectivity to CH_3OH and STY for series of UiO-66 MOFs after 25 h. Taken with permission from ref. [92] Copyright 2020 from MDPI under an open access Creative Commons CC BY 4.0 license.

4. Theoretical calculations on MOFs as catalysts for CH_3OH synthesis from CO_2

As just commented, calculations on active site models can provide detailed understanding on the influence of compositional and structural parameters on the reaction. The periodic structure of MOFs is particularly suited for these calculations, although the number of atoms of the models and the calculation cost in MOFs are usually very high. Development of single-site heterogeneous catalysts has become one of the strategies to achieve highly efficient catalytic processes.[93,94] In one of the earliest precedents applying density functional theory (DFT) calculations to gain understanding on the mechanism of CO_2 hydrogenation on MOFs, Cu-alkoxide-functionalized MOF-5 was found to be a suitable catalyst for CO_2 hydrogenation to HCOOH.[95] Furthermore, UiO-67-supported molecular iridium complex catalyst was also designed for CO_2 hydrogenation to HCOOH.[96] In addition, MIL-101-supported Pt single-atom catalyst was synthesized and found to be more active and selective for CO_2 hydrogenation to CH_3OH than the counterpart having Pt nanocrystals.[97] These results encouraged to develop N-heterocyclic carbene (NHC) of coinage metal hydrides M(I)-H (M=Cu, Ag, and Au) anchored to the UiO-68 organic linker (Figure 15).[98] The activity of UiO-68 decorated with NHC–M(I)–H was studied as a single site catalyst for CO_2 hydrogenation to CH_3OH by DFT calculations. Detailed investigations on this solid revealed a three-stage sequential mechanism for CH_3OH formation through the intermediacy of HCOOH and HCHO. Furthermore, these calculations have led to the conclusion that UiO-68 decorated with NHC–Cu(I)–H should perform better compared to other Ag and Au analogs. These calculations have proposed three descriptors of the catalyst performance based on their linear relationships for the Gibbs energy barrier of CO_2 hydrogenation to HCOO intermediate with them. The first descriptor is the natural bond orbital charge of the hydride in NHC–M(I)–H. The second one is on the electronegativity of M. The third proposed indicator of catalyst performance on CH_3OH

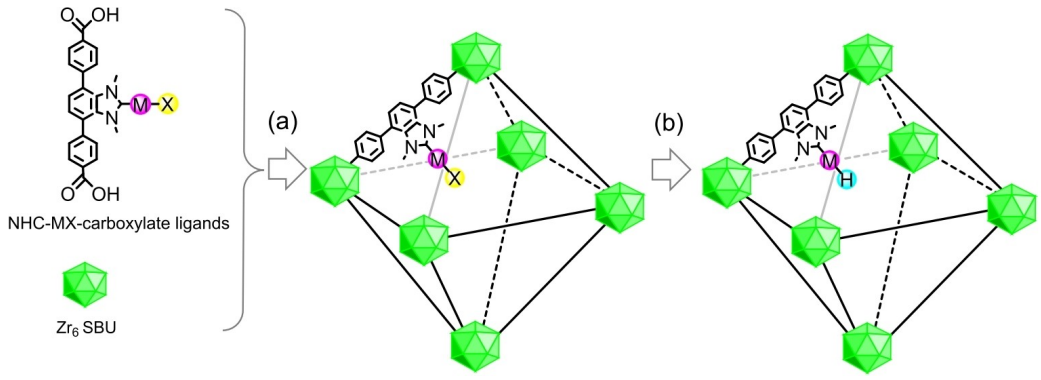

Figure 15. (a) Modified UiO-68 decorated with NHC–M(I)–X prepared from Zr_6 secondary building units and NHC–MX-carboxylate ligands (X=Cl, OH, etc.); (b) Further modification of UiO-68 with the generation of NHC–M(I)–H either by reacting M(I)–X with H_2 or with hydride donors such as silanes and pinacolborane. Taken with permission from ref. [98] Copyright 2021 American Chemical Society.

synthesis is the gap between the lowest unoccupied molecular orbital of CO_2 and the highest occupied molecular orbital of the catalyst. These theoretical findings should be useful to design MOF-based catalysts for CO_2 hydrogenation reaction and need experimental data to validate them. On the other hand, while descriptors are an oversimplification compared to the full mechanistic study, they can be computed at much lower cost and can be very useful to rationalize the key steps in the process and predict further directions for the experimental work.

In another report, a MOF with *frustrated Lewis acid-base pair*, namely, UiO-67-$(NBF_2)_4$ in which BF_2 units are the Lewis acid and N atoms are the basic sites was prepared and its activity was theoretically predicted using DFT calculations for the CO_2 hydrogenation to CH_3OH.[99] The leading concept in the design was that in this type of solids the *frustrated Lewis acid-base pair* could promote the heterolytic dissociation of H_2 preferentially to CO_2 chemisorption, thus avoiding the poisoning of active sites. This concept was supported by calculations that predict the heterolytic dissociation of H_2 into H^- and H^+ bound to Lewis acid and base sites, respectively. Therefore, this facile heterolytic H_2 dissociation facilitates a series of simultaneous transfer of three hydrogens to CO_2 to produce CH_3OH. Since *frustrated Lewis acid base pairs* in homogeneous solution are well established catalysts for CO_2 activation and this concept has been recently implemented in MOFs,[100] it can be expected that it is widely applied for the selective CO_2 hydrogenation to CH_3OH, particularly after realizing that *frustrated Lewis acid-base pairs* in MOFs could be more general than expected and related to the presence of defects.[100]

In one of the few existing examples, Jiang and coworkers have reported detailed DFT studies using a defective UiO-66 lacking some linkers and the resulting defects acting as a *frustrated Lewis acid-base pairs* promoting the hydrogenation of CO_2 to CH_3OH.[101] The defective UiO-66 model with *frustrated Lewis acid-base pairs* was found to be an efficient catalyst for CO_2 hydrogenation to CH_3OH. These calculations have shown the possible sequential steps for the conversion of CO_2 to CH_3OH through HCOOH and HCHO intermediates. These defective MOFs with *frustrated Lewis acid-base pairs* can promote the heterolytic dissociation of H_2 affording proton and hydride as the crucial step in this mechanism of CO_2 hydrogenation. These theoretical calculations should be considered to develop advanced MOF materials with well-defined defective sites for this reaction. It should be interesting to note that MOFs with *frustrated Lewis acid-base pair* sites for heterogeneous catalysis have attracted up to now limited interest, although recent proposals suggest that this activation mechanism could be more general than expected.[100]

In another precedent of theoretical studies, quantum mechanical calculations using periodic density functionals have been performed to examine the quantitative effects of missing linkers at the Cu–Zr node interface in Cu_n@UiO-66 in the activation of H_2 and CO_2 to produce CH_3OH.[102] These studies have shown that catalytic efficiency and product selectivity are highly influenced by the presence and density of linker defects. Further, these defective sites diminish the steric hindrance, facilitating easy access to the catalytic interfacial sites, resulting in the generation of vacancy sites on the Zr ions. However, too many missing linker defects in the UiO-66 structure are detrimental, since CO_2 establishes stronger binding with Zr node than at interfacial sites, thus impeding CO_2 hydrogenation. An optimum number of missing linkers about 5–7 per unit cell was predicted to achieve the highest catalytic efficiency.

5. Conclusions and Future Prospects

The above examples have shown that the use of MOFs as gas phase catalysts for CH_3OH synthesis from CO_2 hydrogenation has recently started, most of the reported studies having appeared in the last five years. Not surprisingly, in view of the remarkable stability of UiO-66, most of the studies have focused on using this type of MOF, either as matrix of Cu and Cu/Zn NPs or even providing the active sites by incorporating atomically dispersed Zn or Cu atoms attached in satellite positions to the metal nodes. In some cases, it has been found that the crystallinity of MOFs does not play a major role, provided that the material still has porosity and surface area. It can be easily predicted that other remarkably stable MOFs such as some of the MIL-series as well as Ti based and other Zr MOFs could also equally be used as an alternative to UiO-66. In fact, stability at the reaction temperature, in the presence of H_2O, under pressure and under operating conditions is the key issue to solve in this area. If this point of structural stability becomes solved, the large versatility of MOFs regarding the design of the active sites at atomic scale with spatial precision in the control of the various components will make MOFs as unbeatable catalysts. Steps in these directions include not only the use of structurally robust MOFs, but also post-synthetic strategies to increase structural stability further, as for example, infusion of Si components to maintain metal nodes and linker in place under reaction conditions. These opens considerably the range of transition metals that can be present in the nodes tuning the electronic density and the energy of the electrons at the Cu–Zn active sites to the most appropriate value for the reaction. Multimetallic nodes are also a direction to explore to increase activity and selectivity, but assistance from computational quantum calculations is needed to rationalize experimental results and to propose the optimal composition. Similarly, insights from computational chemistry on the role of the cage-structure, the density of missing linker and the Lewis acidity of MOFs on CO_2 adsorption and activation will be very valuable.

Besides the metal node, also the linker could play several roles. One of these could be modulating the electronic density of the nodes by inductive effects pulling from or donating the electrons to the nodes as it has been shown in the liquid phase conditions.[103] Furthermore, these ligands can also have substituents that can interact with embedded metal NPs providing a suitable stabilization and tuning the polarity environment.

Regarding polarity and hydrophilicity, it must be considered that water is a reaction product. Therefore, generation of a hydrophobic environment around the active sites could favour the reaction as it has been shown in the liquid phase where hydrophobic zeolites are used to shift reaction equilibrium when water is a product.[104] In any case, realizing the temperature compatibility window between CH_3OH synthesis from CO_2 and MOF as gas phase catalysts opens a wide range of explored possibilities that could result in a definite catalyst that could bring selective CO_2 hydrogenation to CH_3OH to a large industrial scale process in the future.

Acknowledgements

Financial support by the Spanish Ministry of Science and Innovation (CEX-2021-001230-S and PDI2021-0126071-OB-CO21 funded by MCIN/AEI/ 10.13039/501100011033) and Generalitat Valenciana (Prometeo 2021/038 and Advanced Materials programme Graphica MFA/2022/023 with funding from European Union NextGenerationEU PRTR-C17.I1). AD is beneficiary of a grant María Zambrano in Universitat Politècnica de València within the framework of the grants for the retraining in the Spanish university system (Spanish Ministry of Universities, financed by the European Union, NextGeneration EU). S.N. thanks the support of Grant PID2021-123856OBI00 funded by MCIN/AEI/10.13039/501100011033 and by ERDF A way of making Europe. The METHASOL project receives funding from the European Union Horizon 2020 research and innovation programme under Grant Agreement N°101022649.

Conflict of Interest

The authors declare no conflict of interest.

Data Availability Statement

The data that support the findings of this study are available from the corresponding author upon reasonable request.

Keywords: CO_2 Hydrogenation · Gas-Phase Catalysis · Heterogeneous Catalysis · Metal-Organic Frameworks · Methanol Synthesis

[1] M. D. Porosoff, B. Yan, J. G. Chen, *Energy Environ. Sci.* **2016**, *9*, 62–73.
[2] A. Álvarez, A. Bansode, A. Urakawa, A. V. Bavykina, T. A. Wezendonk, M. Makkee, J. Gascon, F. Kapteijn, *Chem. Rev.* **2017**, *117*, 9804–9838.
[3] Z. Chen, N. Youming, Z. Yuchun, W. Fuli, Z. Ziqiao, W. Yingxu, Z. Wenliang, L. Zhongmin, *Angew. Chem. Int. Ed.* **2018**, *57*, 12549–12553.
[4] S. Ilias, A. Bhan, *ACS Catal.* **2013**, *3*, 18–31.
[5] N. A. M. Razali, K. T. Lee, S. Bhatia, A. R. Mohamed, *Renewable Sustainable Energy Rev.* **2012**, *16*, 4951–4964.
[6] W. Wang, S. Wang, X. Ma, J. Gong, *Chem. Soc. Rev.* **2011**, *40*, 3703–3727.
[7] X. Chen, C. Li, M. Graetzel, R. Kostecki, S. S. Mao, *Chem. Soc. Rev.* **2012**, *41*, 7909–7937.
[8] E. L. Kunkes, F. Studt, F. Abild-Pedersen, R. Schloegl, M. Behrens, *J. Catal.* **2015**, *328*, 43–48.
[9] H. Wilmer, T. Genger, O. Hinrichsen, *J. Catal.* **2003**, *215*, 188–198.
[10] R. van den Berg, G. Prieto, G. Korpershoek, L. I. van der Wal, A. J. van Bunningen, S. Laegsgaard-Joergensen, P. E. de Jongh, K. P. de Jong, *Nat. Commun.* **2016**, *7*, 13057.
[11] F. C. Meunier, *Angew. Chem. Int. Ed.* **2011**, *50*, 4053–4054.
[12] S. V. Didziulis, K. D. Butcher, S. L. Cohen, E. I. Solomon, *J. Am. Chem. Soc.* **1989**, *111*, 7110–7123.
[13] J. Hu, L. Yu, J. Deng, Y. Wang, K. Cheng, C. Ma, Q. Zhang, W. Wen, S. Yu, Y. Pan, J. Yang, H. Ma, F. Qi, Y. Wang, Y. Zheng, M. Chen, R. Huang, S. Zhang, Z. Zhao, J. Mao, X. Meng, Q. Ji, G. Hou, X. Han, X. Bao, Y. Wang, D. Deng, *Nat. Catal.* **2021**, *4*, 242–250.
[14] B. Qin, S. Li, *Phys. Chem. Chem. Phys.* **2020**, *22*, 3390–3399.
[15] J. Ye, C. Liu, D. Mei, Q. Ge, *ACS Catal.* **2013**, *3*, 1296–1306.
[16] L. Wang, Y. Dong, T. Yan, Z. Hu, A. A. Jelle, D. M. Meira, P. N. Duchesne, J. Y. Y. Loh, C. Qiu, E. E. Storey, Y. Xu, W. Sun, M. Ghoussoub, N. P. Kherani, A. S. Helmy, G. A. Ozin, *Nat. Commun.* **2020**, *11*, 2432.
[17] J. Ye, C. Liu, Q. Ge, *J. Phys. Chem. C* **2012**, *116*, 7817–7825.
[18] M. Zhang, M. Dou, Y. Yu, *Appl. Surf. Sci.* **2018**, *433*, 780–789.
[19] P. Wu, B. Yang, *Catal. Sci. Technol.* **2019**, *9*, 6102–6113.
[20] H. Jiang, J. Lin, X. Wu, W. Wang, Y. Chen, M. Zhang, *J. CO2 Util.* **2020**, *36*, 33–39.
[21] M. Dou, M. Zhang, Y. Chen, Y. Yu, *New J. Chem.* **2018**, *42*, 3293–3300.
[22] N. Rui, Z. Wang, K. Sun, J. Ye, Q. Ge, C. Liu, *Appl. Catal. B* **2017**, *218*, 488–497.
[23] K. Lee, U. Anjum, T. P. Araújo, C. Mondelli, Q. He, S. Furukawa, J. Perez-Ramírez, S. M. Kozlov, N. Yan, *Appl. Catal. B* **2022**, *304* 120994.
[24] M. D. Porosoff, B. Yan, J. G. Chen, *Energy Environ. Sci.* **2016**, *9*, 62–73.
[25] I. Ud Din, M. S. Shaharun, M. A. Alotaibi, A. I. Alharthi, A. Naeem, *J. CO2 Util.* **2019**, *34*, 20–33.
[26] Y. Yang, M. G. White, P. Liu, *J. Phys. Chem. C* **2012**, *116*, 248–256.
[27] V. D. B. C. Dasireddy, S. S. Neja, L. Blaz, *J. CO2 Util.* **2018**, *28*, 189–199.
[28] J. Toyir, P. Ramirez de la Piscina, J. L. G. Fierro, N. Homs, *Appl. Catal. B* **2001**, *34*, 255–266.
[29] R. Guil-López, N. Mota, J. Llorente, E. Millán, B. Pawelec, J. L. G. Fierro, R. M. Navarro, *Materials* **2019**, *12*, 3902.
[30] A. Corma, H. García, F. X. Llabrés, I. Xamena, *Chem. Rev.* **2010**, *110*, 4606–4655.
[31] L. Zhu, X.-Q. Liu, H.-L. Jiang, L.-B. Sun, *Chem. Rev.* **2017**, *117*, 8129–8176.
[32] A. Dhakshinamoorthy, Z. Li, H. Garcia, *Chem. Soc. Rev.* **2018**, *47*, 8134–8172.
[33] B. Li, M. Chrzanowski, Y. Zhang, S. Ma, *Coord. Chem. Rev.* **2016**, *307*, 106–129.
[34] D. Li, H.-Q. Xu, L. Jiao, H.-L. Jiang, *EnergyChem* **2019**, *1*, 100005.
[35] Q. Wang, D. Astruc, *Chem. Rev.* **2020**, *120*, 1438–1511.
[36] K.-G. Liu, F. Bigdeli, A. Panjehpour, A. Larimi, A. Morsali, A. Dhakshinamoorthy, H. Garcia, *Coord. Chem. Rev.* **2023**, *493*, 215257.
[37] A. Dhakshinamoorthy, A. M. Asiri, H. García, *Trends Chem.* **2020**, *2*, 454–466.
[38] Y.-Z. Chen, R. Zhang, L. Jiao, H.-L. Jiang, *Coord. Chem. Rev.* **2018**, *362*, 1–23.

[39] N. Stock, S. Biswas, *Chem. Rev.* **2012**, *112*, 933–969.
[40] J. L. C. Rowsell, O. M. Yaghi, *Microporous Mesoporous Mater.* **2004**, *73*, 3–14.
[41] P. Valvekens, F. Vermoortele, D. De Vos, *Catal. Sci. Technol.* **2013**, *3*, 1435–1445.
[42] J. Gascon, U. Aktay, M. D. Hernandez-Alonso, G. P. M. van Klink, F. Kapteijn, *J. Catal.* **2009**, *261*, 75–87.
[43] Q. Sun, Z. Dai, X. Meng, L. Wang, F.-S. Xiao, *ACS Catal.* **2015**, *5*, 4556–4567.
[44] J. Mehta, N. Bhardwaj, S. K. Bhardwaj, K.-H. Kim, A. Deep, *Coord. Chem. Rev.* **2016**, *322*, 30–40.
[45] J. Liang, Z. Liang, R. Zou, Y. Zhao, *Adv. Mater.* **2017**, *29*, 1701139.
[46] C. Janiak, *Dalton Trans.* **2003**, *3*, 2781–2804.
[47] C. Wang, B. An, W. Lin, *ACS Catal.* **2019**, *9*, 130–146.
[48] Y.-B. Huang, J. Liang, X.-S. Wang, R. Cao, *Chem. Soc. Rev.* **2017**, *46*, 126–157.
[49] C. Gao, F. Lyu, Y. Yin, *Chem. Rev.* **2021**, *121*, 834–881.
[50] H. Liu, Y. Liu, Y. Li, Z. Tang, H. Jiang, *J. Phys. Chem. C* **2010**, *114*, 13362–13369.
[51] Y. Jin, Q. Zhang, Y. Zhang, C. Duan, *Chem. Soc. Rev.* **2020**, *49*, 5561–5600.
[52] A. Iliescu, J. J. Oppenheim, C. Sun, M. Dinca, *Chem. Rev.* **2023**, *123*, 6197–6232.
[53] I. D. Din, M. Usman, S. Khan, A. Helal, M. A. Alotaibi, A. I. Alharthi, G. Centi, *J. CO2 Util.* **2021**, *43*, 101361.
[54] L. Feng, K.-Y. Wang, G. S. Day, M. R. Ryder, H.-C. Zhou, *Chem. Rev.* **2020**, *120*, 13087–13133.
[55] H. Leclerc, A. Vimont, J.-C. Lavalley, M. Daturi, A. D. Wiersum, P. L. Llwellyn, P. Horcajada, G. Férey, C. Serre, *Phys. Chem. Chem. Phys.* **2011**, *13*, 11748–11756.
[56] S. Wuttke, P. Bazin, A. Vimont, C. Serre, Y.-K. Seo, Y. K. Hwang, J.-S. Chang, G. Frey, M. Daturi, *Chem. Eur. J.* **2012**, *18*, 11959–11967.
[57] A. Vimont, J.-M. Goupil, J.-C. Lavalley, M. Daturi, S. Surblé, C. Serre, F. Millange, G. Férey, N. Audebrand, *J. Am. Chem. Soc.* **2006**, *128*, 3218–3227.
[58] G. C. Shearer, S. Chavan, S. Bordiga, S. Svelle, U. Olsbye, K. P. Lillerud, *Chem. Mater.* **2016**, *28*, 3749–3761.
[59] M. Kandiah, M. H. Nilsen, S. Usseglio, S. Jakobsen, U. Olsbye, M. Tilset, C. Larabi, E. A. Quadrelli, F. Bonino, K. P. Lillerud, *Chem. Mater.* **2010**, *22*, 6632–6640.
[60] K. S. Park, Z. Ni, A. P. Côté, J. Y. Choi, R. Huang, F. J. Uribe-Romo, H. K. Chae, M. O'Keeffe, O. M. Yaghi, *Proc. Natl. Acad. Sci. USA* **2006**, *103*, 10186–10191.
[61] M. Behrens, F. Studt, I. Kasatkin, S. Kuehl, M. Haevecker, F. Abild-Pedersen, S. Zander, F. Girgsdies, P. Kurr, B.-L. Kniep, M. Tovar, R. W. Fischer, J. K. Norskov, R. Schloegl, *Science* **2012**, *336*, 893–897.
[62] M. Hus, V. D. B. C. Dasireddy, N. S. Stefancic, B. Likozar, *Appl. Catal. B* **2017**, *207*, 267–278.
[63] M. Hus, D. Kopac, B. Likozar, *ACS Catal.* **2019**, *9*, 105–116.
[64] R. Gaikwad, H. Reymond, N. Phongprueksathat, P. Rudolf von Rohr, A. Urakawa, *Catal. Sci. Technol.* **2020**, *10*, 2763–2768.
[65] T. Stolar, A. Prasnikar, V. Martinez, B. Karadeniz, A. Bjelic, G. Mali, T. Frisčic, B. Likozar, K. Uzarevic, *ACS Appl. Mater. Interfaces* **2021**, *13*, 3070–3077.
[66] Y. Wang, S. Kattel, W. Gao, K. Li, P. Liu, J. G. Chen, H. Wang *Nat. Commun.* **2019**, *10*, 1166.
[67] J. Wang, G. Li, Z. Li, C. Tang, Z. Feng, H. An, H. Liu, T. Liu, C. Li, *Sci. Adv.* **2017**, *3*, e1701290.
[68] J. Zhang, B. An, Z. Li, Y. Cao, Y. Dai, W. Wang, L. Zeng, W. Lin, C. Wang, *J. Am. Chem. Soc.* **2021**, *143*, 8829–8837.
[69] B. Rungtaweevoranit, J. Baek, J. R. Araujo, B. S. Archanjo, K. M. Choi, O. M. Yaghi, G. A. Somorjai, *Nano Lett.* **2016**, *16*, 7645–7649.
[70] Y. Zhu, J. Zheng, J. Ye, Y. Cui, K. Koh, L. Kovarik, D. M. Camaioni, J. L. Fulton, D. G. Truhlar, M. Neurock, C. J. Cramer, O. Y. Gutiérrez, J. A. Lercher, *Nat. Commun.* **2020**, *11*, 5849.
[71] E. S. Gutterød, A. Lazzarini, T. Fjermestad, G. Kaur, M. Manzoli, S. Bordiga, S. Svelle, K. P. Lillerud, E. Skulason, S. Øien-Ødegaard, A. Nova, U. Olsbye, *J. Am. Chem. Soc.* **2020**, *142*, 999–1009.
[72] E. S. Gutterød, S. H. Pulumati, G. Kaur, A. Lazzarini, B. G. Solemsli, A. E. Gunnæs, C. Ahoba-Sam, M. E. Kalyva, J. A. Sannes, S. Svelle, E. Skulason, A. Nova, U. Olsbye, *J. Am. Chem. Soc.* **2020**, *142*, 17105–17118.
[73] M. S. Frei, C. Mondelli, A. Cesarini, F. Krumeich, R. Hauert, J. A. Stewart, D. Curulla Ferré, J. Pérez-Ramírez, *ACS Catal.* **2020**, *10*, 1133–1145.
[74] S. Kattel, P. Liu, J. G. Chen, *J. Am. Chem. Soc.* **2017**, *139*, 9739–9754.
[75] O. Martin, A. J. Martín, C. Mondelli, S. Mitchell, T. F. Segawa, R. Hauert, C. Drouilly, D. Curulla-Ferré, J. Pérez-Ramírez, *Angew. Chem. Int. Ed.* **2016**, *55*, 6261–6265.
[76] G. Li, S. Zhao, Y. Zhang, Z. Tang, *Adv. Mater.* **2018**, *30*, 1800702.
[77] S. Kattel, P. J. Ramírez, J. G. Chen, J. A. Rodriguez, P. Liu, *Science* **2017**, *355*, 1296–1299.
[78] C. Temvuttirojn, Y. Poo-arporn, N. Chanlek, C. K. Cheng, C. C. Chong, J. Limtrakul, T. Witoon, *Ind. Eng. Chem. Res.* **2020**, *59*, 5525–5535.
[79] C. Zhou, J. Shi, W. Zhou, K. Cheng, Q. Zhang, J. Kang, Y. Wang, *ACS Catal.* **2020**, *10*, 302–310.
[80] J. Zhang, B. An, Y. Cao, Z. Li, J. Chen, X. He, C. Wang, *ACS Appl. Energ. Mater.* **2021**, *4*, 13567–13574.
[81] C. Wang, M. Kosari, S. Xi, H. C. Zeng, *Adv. Funct. Mater.* **2023**, *33*, 2212478.
[82] H. Kobayashi, J. M. Taylor, Y. Mitsuka, N. Ogiwara, T. Yamamoto, T. Toriyama, S. Matsumurad, H. Kitagawa, *Chem. Sci.* **2019**, *10*, 3289–3294.
[83] C.-S. Li, G. Melaet, W. T. Ralston, K. An, C. Brooks, Y. Ye, Y.-S. Liu, J. Zhu, J. Guo, S. Alayoglu, G. A. Somorjai, *Nat. Commun.* **2015**, *6*, 6538.
[84] Y. Mitsuka, N. Ogiwara, M. Mukoyoshi, H. Kitagawa, T. Yamamoto, T. Toriyama, S. Matsumura, M. Haneda, S. Kawaguchi, Y. Kubota, H. Kobayashi, *Angew. Chem. Int. Ed.* **2021**, *60*, 22283–22288.
[85] T. Phongamwong, U. Chantaprasertporn, T. Witoon, T. Numpilai, Y. Poo-arporn, W. Limphirat, W. Donphai, P. Dittanet, M. Chareonpanich, J. Limtrakul, *Chem. Eng. J.* **2017**, *316*, 692–703.
[86] M. Behrens, S. Zander, P. Kurr, N. Jacobsen, J. Senker, G. Koch, T. Ressler, R. W. Fischer, R. Schloegl, *J. Am. Chem. Soc.* **2013**, *135*, 6061–6068.
[87] J. Yu, G. Chen, Q. Guo, X. Guo, P. D. Costa, D. Mao, *Fuel* **2022**, *324*, 124694.
[88] G. Bonura, M. Cordaro, L. Spadaro, C. Cannilla, F. Arena, F. Frusteri, *Appl. Catal. B* **2013**, *140–141*, 16–24.
[89] J. Wang, S.-m. Lu, J. Li, C. Li, *Chem. Commun.* **2015**, *51*, 17615–17618.
[90] M. Zhong, X. Zhang, Y. Zhao, C. Li, Q. Yang, *Green Chem.* **2015**, *17*, 1702–1709.
[91] B. An, J. Zhang, K. Cheng, P. Ji, C. Wang, W. Lin, *J. Am. Chem. Soc.* **2017**, *139*, 3834–3840.
[92] M. Stawowy, R. Ciesielski, T. Maniecki, K. Matus, R. Łuzny, J. Trawczynski, J. Silvestre-Albero, A. Łamacz, *Catalysts* **2020**, *10*, 39.
[93] J. Zhao, S. Ji, C. Guo, H. Li, J. Dong, P. Guo, D. Wang, Y. Li, F. D. Toste, *Nat. Catal.* **2021**, *4*, 523–531.
[94] C. Copéret, *Nat. Energy* **2019**, *4*, 1018–1024.

[95] T. Maihom, S. Wannakao, B. Boekfa, J. Limtrakul, *J. Phys. Chem. C* **2013**, *117*, 17650–17658.
[96] B. An, L. Zeng, M. Jia, Z. Li, Z. Lin, Y. Song, Y. Zhou, J. Cheng, C. Wang, W. Lin *J. Am. Chem. Soc.* **2017**, *139*, 17747–17750.
[97] Y. Chen, H. Li, W. Zhao, W. Zhang, J. Li, W. Li, X. Zheng, W. Yan, W. Zhang, J. Zhu, R. Si, J. Zeng, *Nat. Commun.* **2019**, *10*, 1885.
[98] K. Yang, J. Jiang, *ACS Appl. Mater. Interfaces* **2021**, *13*, 58723–58736.
[99] J. Ye, J. K. Johnson, *Catal. Sci. Technol.* **2016**, *6*, 8392–8405.
[100] A. Dhakshinamoorthy, A. M. Asiri, H. García, *Chem. Eur. J.* **2023**, *29*, e202204016.
[101] K. Yang, J. Jiang, *J. Mater. Chem. A* **2020**, *8*, 22802–22815.
[102] J. Ye, M. Neurock, D. G. Truhlar, *J. Phys. Chem. C* **2022**, *126*, 13157–13167.
[103] A. Santiago-Portillo, M. Cabrero-Antonino, M. Alvaro, S. Navalón, H. García, *Chem. Eur. J.* **2019**, *25*, 9280–9286.
[104] Q. Zhang, J. Yu, A. Corma, *Adv. Mater.* **2020**, *32*, 2002927.

Manuscript received: August 3, 2023
Accepted manuscript online: October 10, 2023
Version of record online: October 27, 2023